Masters Theses   Graduate School

8-2015

Establishing a Chronology of Late Quaternary Glacial Advances in the Cordillera de Talamanca, Costa Rica

Rebecca Susan Potter
University of Tennessee - Knoxville, rpotter6@vols.utk.edu

Follow this and additional works at: https://trace.tennessee.edu/utk_gradthes

Part of the Geology Commons, Geomorphology Commons, Glaciology Commons, Other Earth Sciences Commons, and the Physical and Environmental Geography Commons

To the Graduate Council:

I am submitting herewith a thesis written by Rebecca Susan Potter entitled "Establishing a Chronology of Late Quaternary Glacial Advances in the Cordillera de Talamanca, Costa Rica." I have examined the final electronic copy of this thesis for form and content and recommend that it be accepted in partial fulfillment of the requirements for the degree of Master of Science, with a major in Geography.

<div align="right">Yingkui Li, Major Professor</div>

We have read this thesis and recommend its acceptance:

Sally P. Horn, Henri Grissino-Mayer

<div align="right">Accepted for the Council:
<u>Carolyn R. Hodges</u></div>

<div align="right">Vice Provost and Dean of the Graduate School</div>

(Original signatures are on file with official student records.)

**Establishing a Chronology of Late Quaternary Glacial Advances
in the Cordillera de Talamanca, Costa Rica**

A Thesis Presented for the
Master of Science
Degree
The University of Tennessee, Knoxville

Rebecca Susan Potter
August 2015

ACKNOWLEDGEMENTS

ABSTRACT

Little research has focused on glacial events in the tropics. Providing an absolute glacial chronology in Costa Rica will build a foundation for future glacial chronologies and paleoclimate reconstructions in the highlands of Central America. Evidence of past glaciation, including moraines and glacial lakes, is preserved within formerly glaciated valleys in the Cordillera de Talamanca. Orvis and Horn (2000) constrained deglaciation ages of the most recent glacial event in the Cordillera de Talamanca based on radiocarbon dates of glacial lake sediments. Radiocarbon ages indicated complete deglaciation after 12.4 ka cal BP but before 9.7 ka cal BP (Orvis and Horn, 2000). This research aims to date the formation ages of moraines using cosmogenic ^{36}Cl [chlorine-36] surface exposure dating. Exposure ages provide absolute age constraints on the timing of glacial events within the Cordillera de Talamanca, Costa Rica. Cosmogenic ^{36}Cl exposure ages indicate a Last Glacial Maximum (LGM) event ~21–18 ka, which is synchronous with the global LGM. Ages also indicate periods of glacial retreat and standstills ~18–10 ka. An elevation and age comparison suggests similar timing and extent of LGM advance between two valleys on opposite sides of the mountain range. These results improve understanding of the timing of glacial events in the tropics, which is of critical importance for reconstructing regional and global climate patterns.

Keywords: late Quaternary, glaciation, Costa Rica, cosmogenic ^{36}Cl surface exposure dating, tropics

TABLE OF CONTENTS

LIST OF TABLES

LIST OF FIGURES

CHAPTER 1

Introduction

Studies on past glaciations have been conducted mainly in the middle and high latitudes (e.g. Swanson and Caffee, 2001; Phillips et al., 2009; Young et al., 2011; Laabs et al., 2013), and little is known about paleo-glaciations in tropical regions. This research examines the timing of glacial events in the Cordillera de Talamanca, Costa Rica. Moraine boulders were sampled for cosmogenic ^{36}Cl nuclide surface exposure dating from the Morrenas and Talari Valleys, two formerly glaciated valleys on the massif surrounding Cerro Chirripó, the highest peak in the Cordillera de Talamanca (3819 m; 9°29'04" N, 83°29'20" W). Combined with previous radiocarbon dates of the most recent glacial event (Orvis and Horn, 2000), this study expands upon the existing glacial chronology in the Cordillera de Talamanca. By developing a better understanding of glacial events in Costa Rica, knowledge of regional and global climate patterns can be improved.

Ken Orvis, with assistance from Sally Horn, Carol Harden, and students, collected samples for cosmogenic ^{36}Cl nuclide surface exposure dating from the Morrenas and Talari Valleys in 1998 (Orvis and Horn, 2000), 2000, and 2001 that provided the material for the present study. When a boulder is exposed at the surface of the Earth through erosive processes or mass movement, cosmic rays interact with elements in the boulder to create cosmogenic nuclides. Measuring the nuclide concentration in a boulder allows researchers to determine how long that boulder has been exposed at the surface. A large nuclide concentration typically indicates a long exposure time. This method has been

1

used for research in glaciation, faults, landslides, and other geological processes or landscapes. For my research, I measured cosmogenic nuclide concentration of boulders atop moraines to determine moraine formation and subsequent retreat from that location to constrain the timing of glacial events in the Morrenas and Talari Valleys.

I wish to test the following hypothesis: glacial events in Costa Rica are synchronous with glacial events in the middle and high latitudes of North and South America. The objective of this thesis work is to determine the timing of glacial events in the Morrenas and Talari Valleys using cosmogenic ^{36}Cl surface exposure dating.

This thesis consists of seven chapters. In Chapter 2, I review the literature on glacial events and chronologies in North, Central, and South America, and methods of cosmogenic isotope surface exposure dating. In Chapter 3, I describe the geographical and environmental setting of the Cordillera de Talamanca, specifically of the Morrenas and Talari Valleys. In Chapter 4, I describe the field and laboratory methods used in cosmogenic ^{36}Cl surface exposure dating, and uncertainties associated with cosmogenic dating. In Chapter 5, I present the results of the cosmogenic ^{36}Cl ages from the Morrenas and Talari Valleys. In Chapter 6, I discuss the cosmogenic ^{36}Cl-based glacial chronology and paleoclimate interpretations. I also compare this chronology with previously published cosmogenic chronologies in Central, South, and North America. In Chapter 7, I conclude my thesis by highlighting key points of the results and discussion, the importance of this research, and future research.

CHAPTER 2

Literature Review

The homogenous climate of the tropics differs from the seasonally varying climate in the mid-to high latitudes (Benn et al., 2005). Because of this homogenous climate, significant changes are observed during periods of low and high frequency climate fluctuations, providing valuable insight on past climate change (Licciardi et al., 2009). Severe denudation within these high-energy tropical regions has inhibited the establishment of high-quality glacial chronologies (Benn et al., 2005). Furthermore, uncertainty exists regarding the climate forcing that drives glacial events in the tropics, especially the interplay among changes in precipitation and temperature.

Currently, many arguments exist concerning which climate factors most influence glacial advance and retreat in the tropics. Hastenrath (2009) argued that in the humid tropics, the ice equilibrium line is more sensitive to temperature variation than to precipitation variation. Lachinet and Seltzer (2002) stated that ELA temperature depressions in Costa Rica during the late Quaternary might be linked to drier climate conditions and the position of the Intertropical Convergence Zone (ITCZ). Orvis and Horn (2000) noted that moisture variation, rather than temperature, may have primarily controlled the late Quaternary glaciation in the Cordillera de Talamanca. They postulated that the oldest and most extensive glacial advance in the Morrenas Valley occurred during a time when climate was simultaneously colder and wetter (Orvis and Horn, 2000). Similar observations have been made in Colombia, where palynological data showed cool and humid conditions during the largest recognized advance (Helmens et al., 1997).

The Morrenas and Talari Valleys are currently free of glaciers, but as in neighboring regions (Thouret et al., 1996, Lachinet and Vazquez-Selem, 2005; Lozano-Garcial and Vazquez-Selem, 2005; Roy and Lachinet, 2010), substantial evidence of past glaciation exists. Previously established glacial chronologies may provide further insight into how variations in precipitation, temperature, oceanic, and atmospheric circulation influenced past climate in the tropics.

2.1 Glacial events in Mexico, Central America, and the Northern Andes

Currently, three mountains in Mexico contain glaciers: Pico de Orizaba, Popocatéptel, and Iztaccíhuatl. These glaciers are unique because of their lower latitudinal position, but little is understood on how they gain and lose mass (Delgado, 1997). Radiocarbon dates on glacial deposits from the La Malinche, Nevado de Toluca, and Iztaccíhuatl volcanoes of the central Mexican upland provide evidence for late Quaternary glacial advances between ~9.6 and 7.5 ka cal BP or older than 12 ka cal BP (Heine, 1994). Ages were relatively consistent for all three volcanoes. Based on cosmogenic [36]Cl ages and tephrochronology, a revised chronology of glacial events was constructed for Iztaccíhuatl volcano. Ages indicated two major glacial advances (Hueyatlaco 1 and 2) between 20 and 14 ka, followed by periods of minor retreat and advance until 1 ka (Vazquez-Selem, 2000; Vazquez-Selem and Heine, 2004; Lozano-Garcial and Vazquez-Selem, 2005). Cosmogenic [36]Cl exposure ages also indicated older and major glacial expansions at ~151–126 ka coinciding with the penultimate glacial maximum in Marine Isotope Stage (MIS) 6 (Martinson et al., 1987; Bush et al., 2009).

Complex glacial fluctuations through the late Quaternary into the early Holocene are partly explained by changes of precipitation and temperature. Heine (1994) argued that Laurentide ice sheet meltwater discharged into the Gulf of Mexico contributed to glacier advances (6 °C lower temperatures) in the Mexican highlands. Thus, rapid glacier retreat at higher latitudes may have facilitated an optimum environment for glaciers to advance at lower latitudes.

Similar to Costa Rica, no modern glaciers exist in the highlands of Guatemala. Geographically, Guatemala lies between Mexico to the north and Honduras and El Salvador to the south. During the Last Glacial Maximum (LGM; 26–18 ka) (Glasser et al., 2011), a ~43 km^2 plateau ice cap existed near Montana San Juan (3784 m) in the Sierra los Cuchumatanes (Roy and Lachinet, 2010). During the LGM, land-surface temperatures dropped 5.4 ± 0.3 °C and SST decreased 2.7 ± 0.5 °C (Ballantyne et al., 2005; Roy and Lachinet, 2010). Sediment cores from Lake Petén Itzá provided evidence that climate was not necessarily dry in this region during the LGM, and the driest period was actually during the Lateglacial (~18–11 ka) (Bush et al., 2009). Large ELA depressions observed in Guatemala were perhaps associated with an increase in moisture from southward digressions of the boreal winter polar air mass (Roy and Lachinet, 2010). Past ELA depressions in Guatemala are similar to Costa Rica (Orvis and Horn, 2000; Lachinet and Seltzer, 2002). Absence of suitable material and chemical dissolution of limestone boulders and glacial features has hindered cosmogenic dating in Guatemala (Roy and Lachinet, 2010; Lachinet and Roy, 2011). Political strife has also slowed research in the region (Caffrey et al., 2011).

Colombia is located south of Costa Rica in the northern Andes of South America. Radiocarbon dates from lake sediments, peat, and paleosols indicated major glacial advances in the eastern Cordillera of Colombia that pre-date the LGM (Helmens et al., 1997). Specifically, in the Bogota area, radiocarbon dates indicated the most extensive glaciations occurred before 40.2 ka cal BP but probably after 45.0 ka cal BP, and between 38.5 ka cal BP and 33.5 ka cal BP (Helmens, 1990; Helmens and Kuhry, 1995; Helmens et al., 1997).

In the Sierra Nevada of the Merida Andes, Venezuela, Carcaillet et al. (2013) constrained the timing of glacial events using cosmogenic [10]Be surface exposure dating. Ages indicated that the largest advance occurred 18.1 ka and five moraine complexes dated between 18.1 and 15.8 ka representing periods of minor advance and retreat during an overall retreat. Ages indicated complete deglaciation ~9.5 ka in the Mucubaji Valley (Carcaillet et al., 2013). This deglaciation age is similar to radiocarbon ages obtained from lake sediment cores in the Morrenas Valley, Costa Rica (Orvis and Horn, 2000).

Throughout the Quaternary, glacial events in Central America and the northern Andes have been controlled by climate fluctuations. Based on tropical ELA depressions, paleo-temperatures in the tropics decreased by 3.3 to 8.4 °C during the LGM (Porter, 2001). This differs from sea-surface temperature (SST) reconstructions by CLIMAP (1981), which showed only marginal temperature changes, perhaps even slight warming, during the LGM in the tropics (Seltzer, 2001). This suggests a potentially steeper temperature lapse rate inland at higher altitudes than observed at sea level. A dominant hypothesis to explain the occurrence of past tropical glaciation is that tropical glaciers may be more sensitive to mean annual temperature variability than precipitation

6

variations (Seltzer, 1994; Kaser and Osmaston, 2002; Seltzer et al., 2002; Benn et al., 2005; Roy and Lachinet, 2010).

2.2 Glacial events in Central and Southern Andes

Extensive glacial studies exist in the Central and Southern Andes. Despite abundant data, the timing and extent of these events remain poorly constrained, especially between the eastern and western slopes of the Andes (Bromley et al., 2009). This inconsistency is believed to be caused by the small-scale, highly variable climate and topography typical of the Andes (Hall et al., 2009). The Andes region contains high-elevation, U-shaped valleys with well-preserved glacial features ideal for cosmogenic nuclide dating (Hall et al., 2009). Furthermore, the extensive range of latitudes and changing climate environments can provide insight into the variation in the timing of glacial events throughout the Andes (Hall et al., 2009).

The Peruvian Andes are located in the northern segment of the mountain chain extending from the middle to northwestern region of South America with well-preserved glacial features. Glacial chronologies established in the Peruvian Andes indicate asynchronous glacial events in different regions. Bromley et al. (2009) established a cosmogenic ^{3}He glacial chronology for Nevado Coropuna (6425 m; 15°33'S, 72°93'W), the largest and tallest volcano in Peru. Ages indicated that glaciers reached their maximum extent between ~25 and 15 ka, coinciding with the global LGM (Bromley et al., 2009). Using cosmogenic ^{10}Be dating, Glasser et al. (2009) dated moraines from the western side of the Andean transect in the Cordillera Blanca, Peru. Contrastingly, LGM moraines were absent in the valley, and they concluded that no significant glacial

advances occurred in the western Cordillera until 16–12 ka due to lack of moisture (Glasser et al., 2009). Smith and Rodbell (2010) also conducted research in the Cordillera Blanca using cosmogenic ^{10}Be dating. Exposure ages indicated at least four periods of glacier stabilization >65 ka, ~65 ka, ~32 ka, and ~18–15 ka (Smith and Rodbell, 2010). They also noted the absence of LGM moraines.

Sediment data from Lake Junin (Peru) indicated maximum glacial extent ~33–22 ka cal BP, while deglaciation may have occurred during the global LGM due to a regionally moist climate (Seltzer et al., 2002). Smith et al. (2005) used cosmogenic ^{10}Be dating in the Lake Junin region and obtained similar results. They found that glaciers reached their maximum expansion as early as ~34 ka, and deglaciation commenced ~21 ka. They related these advances (and possibly earlier advances) to sharp depressions of SSTs in the east equatorial Pacific (Lea et al., 2000; Smith et al., 2005).

Smith et al. (2009) established a cosmogenic ^{36}Cl chronology for the Western Cordillera, Bolivia. Ages indicated that the largest glacial advance occurred during the Lateglacial (16.9–11.3 ka). Moraines down valley may provide evidence of older, more extensive glaciations, but could not be sampled because they were overlaid or crosscut by younger moraines.

Past climate fluctuations observed in the central and southern Andes seemed to have considerably influenced regional glacial patterns. Some research has determined maximum glacial extent occurred pre-LGM (Seltzer et al., 2002; Smith et al., 2005), while other research has indicated maximum extent occurred during the Lateglacial (Glasser et al., 2009; Smith et al., 2009). This variability has been ascribed to moisture availability. In addition, research has suggested that the North Atlantic ice-melt

8

oscillation lowered SSTs, which decreased inland temperatures in the northern and southern Andes.

2.3 Glacial events in the United States

In the United States, both synchronous and asynchronous timing of past glacial events has been observed. Similar to South America, preservation of moraines and multi-proxy dating methods have allowed researchers to identify the forcing mechanisms and timing of glacial advances and retreats. Chronologies of glacial events in North America commonly date as far back as MIS 6 (~151–126 ka) (Martinson et al., 1987; Bush et al., 2009). However, more recent glaciations have overridden some older moraines, making dating difficult.

In the western United States, several cosmogenic [10]Be glacial chronologies have been established. In the Arkansas River Basin, Colorado, cosmogenic [10]Be ages indicated glaciers reached maximum extent asynchronously (compared with other western U.S. chronologies) at 22.4 ka, 19.2 ka, 17.8 ka, and 15.8 ka (Young et al., 2011). However, glacial retreat was synchronous between ~16 and 15 ka (Young et al., 2011). They noted that while climate change is almost always the primary factor in glacier change, the asynchronous onset of glaciation observed in the western U.S. might be a result of variable geographic location and glacial characteristics (Young et al., 2011).

Laabs et al. (2013) sampled 29 boulders for [10]Be exposure dating from the Ruby Mountains, Great Basin, USA. Two distinct glacial events were observed. Ages indicated that the older advance began retreating before ~20.5 ka after reaching maximum extent, and the youngest retreat was complete by ~14.8 ka (Laabs et al., 2013). The timing of

these events was broadly synchronous with neighboring regions including the Rocky Mountains and the Sierra Nevada (Laabs et al., 2013). The cosmogenic chronologies established by Young et al. (2011) and Laabs et al. (2013) indicated extensive and/or final LGM deglaciation occurred ~16–15 ka. However, they both stated that caution must be taken when ascribing regionally uniform ages to glacial events in the western United States. Spatially, the Great Basin region is just one of several unique North American environments where glacial events may have been influenced by contrasting factors.

In the Sierra Nevada, California, Rood et al. (2011) developed a glacial chronology using cosmogenic [10]Be dating. In contrast to previously mentioned studies, they were able to identify and date MIS 6 moraines. A total of 115 [10]Be ages from this study indicated LGM retreat began 18.8 ka, and the penultimate glaciation occurred ~145 ka (Rood et al., 2011). LGM events were synchronous on the east and west-facing slopes of the Sierra Nevada. However, ages showed that local LGM retreat occurred several thousand years prior to retreat observed elsewhere in the western U.S. (Rood et al., 2011). Cosmogenic [36]Cl ages from the eastern Sierra Nevada show similar results (Phillips et al., 2009).

In contrast to the mid-to high latitudinal continental region of North America, the climate of the Hawaiian Islands is somewhat comparable to Costa Rica. Cosmogenic [36]Cl nuclide ages from Mauna Kea, Hawaii, indicated two glacial events (Pigati et al., 2008). The older Makanaka glaciation retreated from its maximum extent ~23 ka, and the younger Makanaka glaciation ~13 ka (Pigati et al., 2008). Pigati et al. (2008) reconstructed precipitation and temperature to observe which conditions were most ideal for glacial onset. They found that a seasonal increase in frequency and intensity of storms

and cold fronts were the primary forcing factors for glacier advance rather than tropical cyclones and trade winds. The precipitation and temperature models showed the older Makanaka glaciation occurred at a time of cooler temperatures and increased precipitation compared to the present climate. The younger Makanaka glaciation occurred during a time of largely increased precipitation (Pigati et al., 2008). Similar to findings in Colombia (Thouret et al., 1996), glaciers in Hawaii were retreating at a time when, globally, many glaciers were reaching their maximum position (Pigati et al., 2008).

Past climate conditions ideal for glacial onset in Hawaii may be comparable to Costa Rica. Within the continental U.S., high spatial variation of topography was the likely factor in regionally observed asynchronous timing of advance and retreat. As previously mentioned, LGM events seemed to be locally synchronous within the Sierra Nevada, but occurred earlier there than in other regions in the western United States (Phillips et al., 2009; Rood et al., 2011). Synchronous timing of retreat was observed in the Rocky Mountain and Great Basin regions (Young et al., 2011; Laabs et al., 2013).

The chronologies discussed above only represent a small fraction of established cosmogenic glacier chronologies in North, Central, and South America. Some chronologies indicated local LGM events to be synchronous with global LGM events, while others were asynchronous. Although the LGM has been commonly accepted as a global-scale cold event, research has shown that glaciers in some regions reached maximum extent before or after this period. Thus, it is important to establish detailed glacial chronologies to better understand past climates on a regional and global scale. My new cosmogenic ^{36}Cl-based glacial chronology for the Cordillera de Talamanca, Costa

Rica, will improve the understanding of the timing and extent of glacial events in the

tropics.

2.4 Cosmogenic ^{36}Cl surface exposure dating

The theory associated with cosmogenic nuclides was developed in the early 20th

century, but the application of cosmogenic nuclides in Earth Sciences is fairly recent. In

the 1930s, researchers discovered that cosmic rays are altered by the Earth's magnetic

field (Dunai, 2010). It was not until the 1980s that geologists and geochronologists

realized the potential of using this method in glacial research (Balco, 2011). Scientists

also use cosmogenic nuclide dating to study volcanic activity, fault movement,

denudation rates, and many more geological processes and landscapes.

Cosmogenic nuclides on Earth evolve from galactic cosmic rays. Cosmic rays are

high-energy, charged particles that penetrate the Earth in every direction and mostly

consist of atomic nuclei (Dunai, 2010). Once these atomic nuclei come into contact with

Earth's atmosphere, the primary cosmic rays generate secondary cosmic rays through

interactions with atmospheric atoms (Dunai, 2010). These atoms, in turn, interact with

rock material at the surface of the Earth where naturally occurring elements within rock

material are altered into isotopically different elements (Figure 1).

Chlorine-36 ($t_{1/2} = 3.01 \times 10^5$ yr) was the first in situ produced nuclide discovered

in rock material (Davis and Schaeffer, 1955; Zreda et al., 1991). Cosmogenic ^{36}Cl

nuclides are produced in rock material through reactions with ^{35}Cl, ^{39}K, and ^{40}Ca when

exposed at Earth's surface to cosmic rays (Zreda et al., 1991). Due to these multiple

reactions, ^{36}Cl is a particularly adaptable nuclide because minerals, such as plagioclase

12
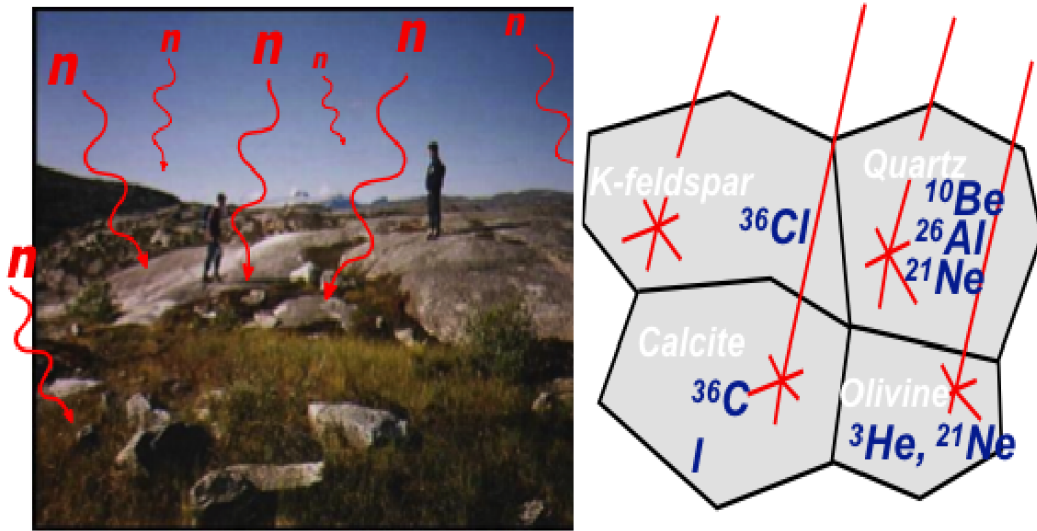
Figure 1: Cosmic rays interacting with naturally occurring elements in boulders (provided by Y. Li; originally created by D. Fabel, A.P. Stroeven, and J. Harbor).

(Ca-rich), calcite (Ca-rich), and orthoclase feldspar (K-rich), are abundant in many rock lithologies (Phillips et al., 1986; Licciardi et al., 2008).

Cosmogenic nuclide dating is beneficial in several ways compared to other dating methods. The age range is larger than radiocarbon dating. Sampling for boulders is relatively straightforward and a wide range of rock types can be dated. However, several disadvantages exist in cosmogenic dating. These include expensive laboratory setup, risk of contamination, and the lack of material suitable for cosmogenic dating at some field sites. Uncertainties also exist with production rates and scaling models used in cosmogenic dating as described below.

Shielding

Dunai (2010) defines shielding as any solid mass that is sufficiently thick to obstruct or diminish the cosmic-ray flux at or near the sampling site. Shielding will have an effect on the cosmic-ray flux and the associated cosmogenic nuclide production at the site. Calculations are commonly used to correct for various shielding factors. Topographic shielding is the most common one when sampling boulders. The surface of a boulder should ideally be laying on a flat and horizontal surface completely exposed to the sky. This allows for a maximum amount of cosmic-ray interaction (Dunai, 2010). Other common shielding factors include surface coverage shielding (vegetation, snow, volcanic ash) and tectonic uplift or subsidence (Dunai, 2010).

Production Rates

The greatest uncertainty in cosmogenic dating involves production rates and how they vary temporally and spatially (Licciardi et al., 2008). The production rate is simply the rate at which naturally occurring elements within rock isotopically change when exposed to cosmic rays. Spatially, production rates tend to increase with latitude and altitude. Temporally, production rates change due to variations in the strength and orientation of the geomagnetic field and solar modulation (Kurz et al., 1990; Pigati and Lifton, 2004; Licciardi et al., 2008). Cosmogenic ^{36}Cl nuclides are unique among other cosmogenic nuclides because they form through reactions with multiple isotopes, primarily ^{35}Cl, ^{39}K, and ^{40}Ca (Licciardi et al., 2008). However, these reactions further complicate the total production of ^{36}Cl because three separate production rates for ^{35}Cl, ^{39}K, and ^{40}Ca must be taken into account rather than a single production rate (Licciardi et al., 2008).

Scaling Factors

Scaling factors are used in calculating production rates for cosmogenic nuclides. Scaling factors quantify how cosmic-ray flux varies with changes in latitude, altitude, and time (Dunai, 2010). Scaling factors used in calculating production rates include coordinate systems and input parameters. Variables included in coordinate systems are geographic and geomagnetic coordinates. Input parameters include atmospheric pressure, geomagnetic field, and solar modulation (Dunai, 2010).

CHAPTER 3

Study Area

The Cordillera de Talamanca is a northwest-southeast trending mountain range in Costa Rica and Panama (Figure 2). Cerro Chirripó (3819 m; 9°29'04" N, 83°29'20" W) is the highest peak in Costa Rica. This study focuses on two formerly glaciated valleys, the Morrenas and Talari Valleys. Glacial features including moraines and glacial lakes are preserved in these two valleys although no modern glaciers exist. Evidence of ice cap coverage is observed in surrounding valleys (Lachinet and Seltzer, 2002). Climate observational data are available from the Cerro Páramo meteorological station (3466 m; 9°33'41" N, 83°45'18" W), located ~30 km west of Cerro Chirripó (Lane et al., 2011). This station recorded a mean annual precipitation of 2581 mm and a mean annual temperature of 8.5 °C between 1971 and 2000 (Instituto Costarricense de Electricidad, unpublished data; Lane et al., 2011). This tropical region is near the 0° isotherm where the annual mean temperature is less variable than the daily mean temperature (Benn et al., 2005).

The Morrenas Valley is a north-northwestern-facing valley adjacent to the Chirripó headwall. Glacial features provide evidence of past glacial events. Within the cirque, glacial lakes and moraines create a hummocky terrain surrounded by valley walls with limited vegetation growth on top of bedrock (Horn et al., 2005). The size of these lakes vary, but the largest measures ~8 ha and 22 m deep (Horn et al., 2005). The gradient of the valley floor steepens down valley from the cirque.

16
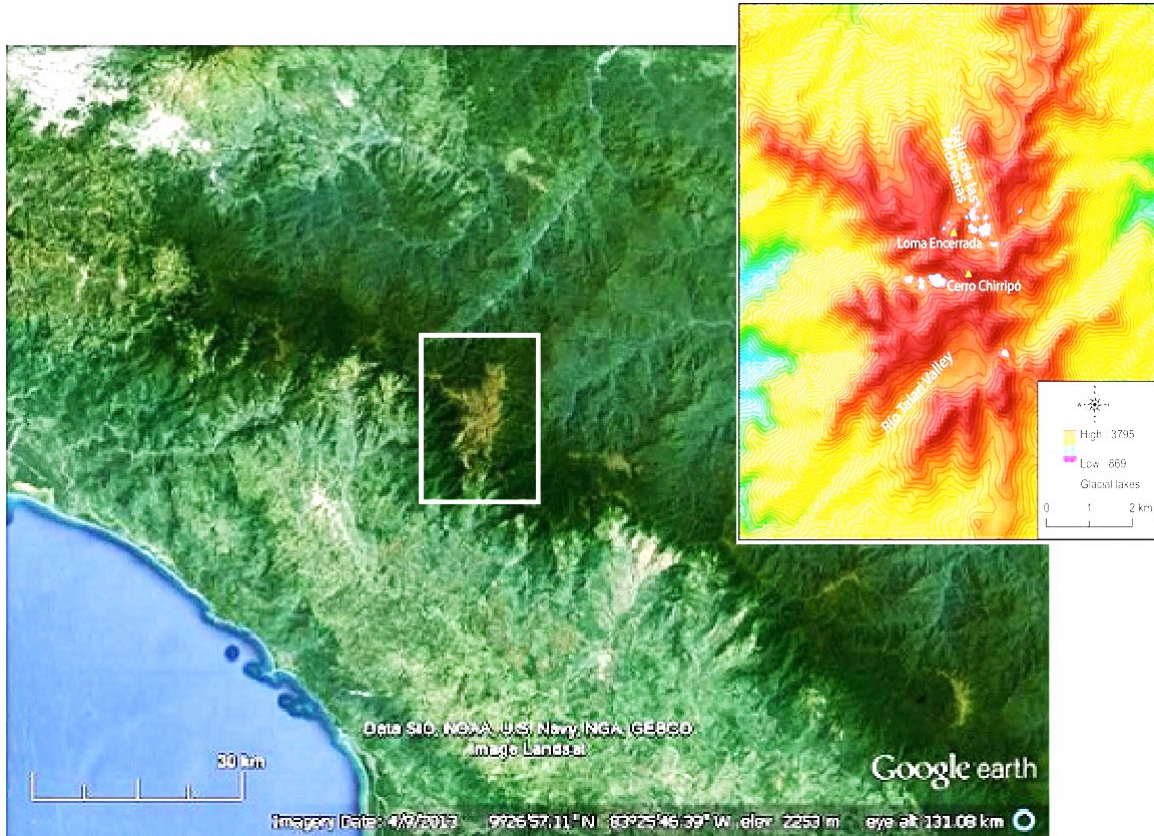
Figure 2: Google Earth image with white border around Cerro Chirripó, Cordillera de Talamanca, Costa Rica. Inset shows a Digital Elevation Model of the study area (created by Y. Li using the 90-m SRTM DEM).

The Talari Valley faces southwest. In contrast to the Morrenas Valley, no glacial lakes are present. Similar to the Morrenas Valley, the cirque has a hummocky terrain and the valley gradient steepens down valley from the cirque. On the northwest side of Suroeste Peak in the upper Talari Valley, freeze-thaw processes have produced solifluction terraces in the ablation till mantling the slope (Lachinet and Seltzer, 2002).

Weyl (1956 a, b) first mentioned evidence of glacial activities near Cerro Chirripó, and Hastenrath (1973) identified specific moraine complexes. Bergoeing (1977) interpreted glacial geomorphology from aerial photographs and Barquero and Ellenberg (1983, 1986) mapped glacial features based field work and aerial photograph analyses. Orvis and Horn (2000) conducted geomorphic analysis of glacial features, reconstructed past ELAs, and cored sediments in glacial lakes of the Morrenas Valley. They mapped four moraine complexes in the Morrenas Valley: Chirripó IV (oldest), III, II, and I (youngest) (Figure 3). Radiocarbon ages from lake sediment cores in the Morrenas Valley indicated that the last advance could correspond in time to the Younger Dryas, with this advance followed by complete deglaciation after 12.4 ka cal BP and before 9.7 ka cal BP (Orvis and Horn, 2000). These ages corresponded to the youngest identified moraine complex (Chirripó I). Orvis and Horn (2000) interpreted the Chirripó II moraine complex to be associated with MIS 2, and tentatively correlated Chirripó III with MIS 4, and Chirripó IV with MIS 6. These assigned MIS stages indicated older, more extensive glaciation down valley from the Chirripó massif, but absolute ages are needed for further investigation (Orvis and Horn, 2000; Lachinet and Vazquez-Selem, 2005). Lachinet and Seltzer (2002) mapped three moraine groups in both the Morrenas and Talari Valleys: Talamanca (oldest), Chirripó, and Talari (youngest). The most extensive moraine
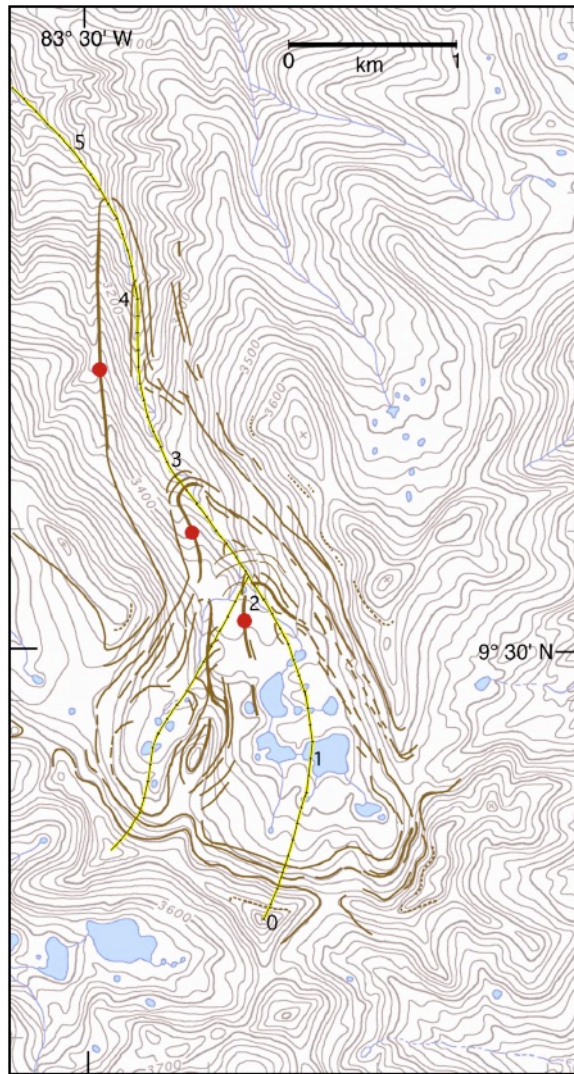
Figure 3: Moraines (heavy lines) and trimlines and other geomorphic evidence (lighter lines) of glacial extents in the Morrenas Valley, north flank of Cerro Chirripó, Cordillera de Talamanca. Dots (red) show origins of sample sets retrieved for cosmogenic nuclide dating (Orvis and Horn, 2000, color version courtesy of K. Orvis).

complex is defined as Chirripó IV (Orvis and Horn, 2000). In the Talari Valley, large lateral moraines ~30 m high are attributed to this extensive moraine group (Lachinet and Seltzer, 2002).

The Chirripó III (Orvis and Horn, 2000) or Chirripó (Lachinet and Seltzer, 2002) moraine complex terminates at ~3300 m in both valleys (Orvis and Horn, 2000; Lachinet and Seltzer, 2002). Large lateral moraines are visible in the Morrenas and Talari Valleys, and a terminal moraine is noted in the Talari Valley (Orvis and Horn, 2000; Lachinet and Seltzer, 2002).

The Chirripó II (Orvis and Horn, 2000) or Talari (Lachinet and Seltzer, 2002) moraine terminus extends to 3300 m in the Talari Valley and 3400 m in the Morrenas Valley. Four moraines are found in the Talari Valley, and one moraine consisting of two separate ridges is located in the Morrenas Valley (Lachinet and Seltzer, 2002).

Slopes above ~3200 m on the Chirripó massif support neotropical páramo vegetation dominated by the dwarf bamboo *Chusquea subtessellata* (Horn, 1989, 1998). Evergreen shrubs, grasses, and herbs grow intermixed with the bamboo. Pollen assemblages in the sediments of Lago de las Morrenas 1, the largest lake in the Morrenas Valley, shows that the valley has been treeless since lake formation ~11 ka cal BP (Horn, 1993). Microscopic and macroscopic charcoal in the lake sediments indicate periodic fires on the massif, set by people or lightning (Horn, 1993; League and Horn, 2000). Stable isotope analyses of glacial lake sediments reveal shifts in moisture availability over the Holocene, with the middle Holocene generally wetter than the early and late Holocene (Lane et al., 2011; Lane and Horn, 2013).

CHAPTER 4

Methods

4.1 Field work

On three expeditions to the Chirripo highlands in February 1998, March 2000, and May 2001, Dr. Kenneth Orvis working with Drs. Sally Horn and Carol Harden, and students Brandon League and Charles Lafon collected boulder samples suitable for cosmogenic ^{36}Cl surface exposure dating. They collected 6 initial samples in 1998 from moraines within the cirque of the Morrenas Valley and 50 samples atop moraines in the Morrenas and Talari Valleys in 2000 and 2001 (Figure 4). A suitable boulder for cosmogenic dating must be in situ, have minimal surface erosion, and be lying on a low-degree slope to assure accurate exposure age. Using a hammer and chisel, approximately 1000 grams of rock material was chipped from the surface of each boulder. Latitude, longitude, and elevation were recorded for each sampled moraine.

Four moraine complexes in the Morrenas Valley, previously mapped by Orvis and Horn (2000), were sampled for this study. In the Morrenas Valley, six boulder samples were collected in 1998 from moraines within the Morrenas cirque, corresponding to the Chirripó I moraine complex, and thirty boulder samples were collected in 2000 from three moraines corresponding to the moraine complexes identified by Orvis and Horn (2000): IV, III, and II (Figure 2). Twenty boulder samples were collected in 2001 from two moraines in the Talari Valley that most likely correspond to the Talamanca moraine complex mapped by Lachinet and Seltzer (2002).

21

Figure 4: (A-F): Sampling boulders for cosmogenic ^{36}Cl surface-exposure dating in the Morrenas and Talari Valleys. (G): Bedrock with glacial striations in the Talari Valley. Photo credits: Carol Harden and Sally Horn

4.2 Cosmogenic ^{36}Cl sample processing

Five of the six samples collected in 1998 were processed in Purdue Rare Isotope

Measurement Laboratory (PRIME) Lab with the support of a seed grant. Y. Li also

processed 9 samples collected in 2000 and 2001 at PRIME Lab in 2012. All other

samples were processed for cosmogenic ^{36}Cl analysis at the cosmogenic sample

preparation lab in the Laboratory of Paleoenvironmental Research at the University of

Tennessee, which I helped set up. The detailed laboratory procedure that I developed

with Dr. Li based on Purdue University protocols is provided in Appendix A. In general,

processing ten ^{36}Cl samples takes 2–3 weeks. For whole-rock ^{36}Cl sample processing,

each boulder sample was crushed up into granular size. The samples were then leached to

remove fine sediment and organic material. After leaching, 15 grams from each sample

was preserved in a vial and sent to Minerals Analytical at the SGS Canada Corporation

for elemental analysis. Elemental analysis is important because ^{36}Cl has multiple reaction

pathways that are included in calculating the production rate. In particular, the

concentrations of important elements (e.g. Li, B, Cl, Cf, Sm, Gd, U, and Th) could affect

the production rate and subsequent exposure age (Phillips et al., 2001; Schimmelpfennig

et al., 2009; Dunai, 2010). During sample processing, ^{35}Cl spike carrier was added to

each sample to measure the ratio of naturally occurring ^{35}Cl to the isotopic ^{36}Cl produced

at the boulder's surface during exposure. Silver nitrate ($AgNO_3$) was then added to each

sample to precipitate silver chloride (AgCl). This silver chloride precipitate contained the

chlorine used to measure isotopic ^{36}Cl/^{35}Cl ratios with accelerator mass spectrometry

(AMS). Samples were then eluted through anion exchange chromatography. This process

filtered out any unwanted or excess material from the sample to assure the purest form of

chloride for final sample preparation. Finally, the samples were loaded into a ^{36}Cl holder

(Cu covered by AgBr) and sent to the PRIME Lab at Purdue University for AMS

measurement.

4.3 Exposure age calculations

Prior to calculating exposure ages, several input values must be calculated using

the AMS results from the PRIME lab and the elemental analysis from Minerals

Analytical at the SGS Canada Corporation. Input values include, but are not limited to,

the ratio of chlorine-35 to chlorine-37, the ratio of chlorine-36 atoms to the total atomic

mass of the sample, and the mass fraction of chlorine-36 (parts per million) in the sample.

The entire set of input variables is provided in Appendix B. Production rate, attenuation

length, and a topographic shielding factor must also be calculated for each sample or site.

The production rate calculation is provided below (Swanson and Caffee, 2001):

$$P = \psi_{Ca}(C_{ca}) + \psi_K(C_K) + \psi_n(\sigma_{35} \, N_{35}/\Sigma\sigma_i N_i)$$

where ψ_K and ψ_{Ca} are the total production rates of ^{36}Cl due to potassium and calcium,

respectively; C_K and C_{ca} are the elemental concentrations of potassium and calcium,

respectively; and ψ_n is the thermal neutron capture rate, which is dependent on the

fraction of neutrons stopped by ^{35}Cl ($\sigma_{35} \, N_{35}/\Sigma\sigma_i N_i$), as determined by the effective cross

sections of ^{35}Cl (σ_{35}) and all other absorbing elements ($\Sigma\sigma$) and their respective

abundances (N_{35} and N_i) (Swanson and Caffee, 2001).

Manual age calculations prove tedious, time demanding, and create higher

potential for human error. For this reason, the online ^{36}Cl Exposure Age Calculator

developed by CRONUS (Cosmic-Ray Produced Nuclide Systematics on Earth Project)

was used (Phillips et al., 2002; Version 1.0; http://web1.ittc.ku.edu:8888/html/latest/cl/).

The CRONUS online calculator includes necessary inputs for an accurate calculation

such as production rate, scaling, topographic shielding factor, elemental concentrations,

and coordinate system. Cosmogenic ^{36}Cl exposure ages were calculated using two scaling

models developed by Desilets and Zreda (Desilets and Zreda, 2003; Desilets et al., 2006)

and Lifton and Sato (Lifton et al., 2008; Sato et al., 2008; Lifton et al., 2014).

4.4 Geo-referencing and topographic shielding

While sampling in the field, the coordinates and elevation of each boulder were

recorded as Octopeque coordinates, a coordinate system local to Costa Rica (Orvis, 2002).

To accurately calculate the topographic shielding and exposure ages, the original

coordinates and elevations were converted into WGS84 coordinates. Using ArcGIS, a set

of control points was extracted between a base map and aerial photographs that contained

the study sites to determine the new coordinates and elevations. Topographic shielding

factors were then calculated in ArcGIS using a digital Shuttle Radar Topography Mission

DEM (90 m resolution) following the method described by Li (2013).

4.5 Uncertainties associated with cosmogenic ^{36}Cl exposure ages

Production rate, shielding, boulder surface erosion, and scaling models all affect

cosmogenic nuclide surface exposure dating. The largest uncertainty in cosmogenic

nuclide dating involves the production rate and how it varies temporally and spatially

(Licciardi et al., 2008). Spatially, production rates tend to increase with latitude and

altitude. Temporally, production rates change due to variations in the strength and

orientation of the geomagnetic field and solar modulation (Kurz et al., 1990; Pigati and

Lifton, 2004; Licciardi et al., 2008). Shielding from topography and possible

sediment/snow cover obstruct or diminish the cosmic-ray flux at or near the sampling site

(Dunai, 2010), reducing cosmogenic nuclide production at the site (a topographic

shielding factor has been considered in the age calculation). Factors incorporated into

scaling models include cosmic-ray flux and the influence of the magnetic fields of Earth

and the Sun (Dunai, 2010). These factors vary with altitude and latitude. Thus, applying

different scaling models can produce different exposure ages. Geomorphic processes,

such as fluvial or mass movement, can result in exposure ages younger or older than the

true exposure age (Ivy-Ochs et al., 2007; Balco, 2011; Applegate et al., 2012). Post-

glacial processes such as boulder toppling or exhumation will reduce nuclide

concentrations and cause the apparent exposure ages to be younger than the formation

age (Applegate et al., 2012). Some boulders might be exposed prior to the moraine

formation, resulting in inheritance. This inheritance causes apparent exposure ages to be

older than the time of the moraine formation (Applegate et al., 2012). Additionally, the

surface of a boulder will inevitably erode through time resulting in uncertainties in

exposure age.

I calculated the changes in the exposure ages using different erosion rate and

scaling model inputs. The absolute and relative differences in ages were derived to

evaluate the uncertainties caused by surface erosion and the scaling model.

CHAPTER 5

Results

In total, forty-eight cosmogenic ^{36}Cl exposure ages were obtained to constrain the timing of glacial events in Cerro Chirripó, Costa Rica (Figure 5; Table 1). I plotted the exposure ages as a probability density function (PDF) to observe age clusters and scatter, and to identify possible outliers (Figure 6) (Li et al., 2014; Chen et al., 2015). The ages were calculated under the assumption of zero surface erosion using the Desilets and Zreda (Desilets and Zreda, 2003; Desilets et al., 2006) scaling model.

5.1 Morrenas Valley

Thirty-three cosmogenic ^{36}Cl nuclide exposure ages of boulders atop moraines provide a constraint on the timing of glacial events in the Morrenas Valley. The Chirripó IV (M4) moraine complex corresponds to the oldest and largest glacial advance in this valley. Boulders were sampled atop this moraine at an elevation of 3310 m. Ages from this moraine range from 48.0 ± 13.0 to 5.1 ± 1.0 ka (*n* = 10). The PDF of M4 ages (Figure 6A) indicates eight of the ten ages cluster around 16.6 ka, and the ages of 5.1 ± 1.0 ka and 48.0 ± 13.0 ka are likely outliers. An exposure age younger than the primary age range of a given moraine likely resulted from that boulder being exposed to the surface after moraine formation due to post-glacial degradation processes. An exposure age older than the age range likely resulted from that boulder being exposed to the surface prior to moraine formation causing inheritance. The Chirripó III (M3) moraine complex is ~0.9 km up-valley from the Chirripó IV (M4) moraine. Boulders were sampled atop this

27
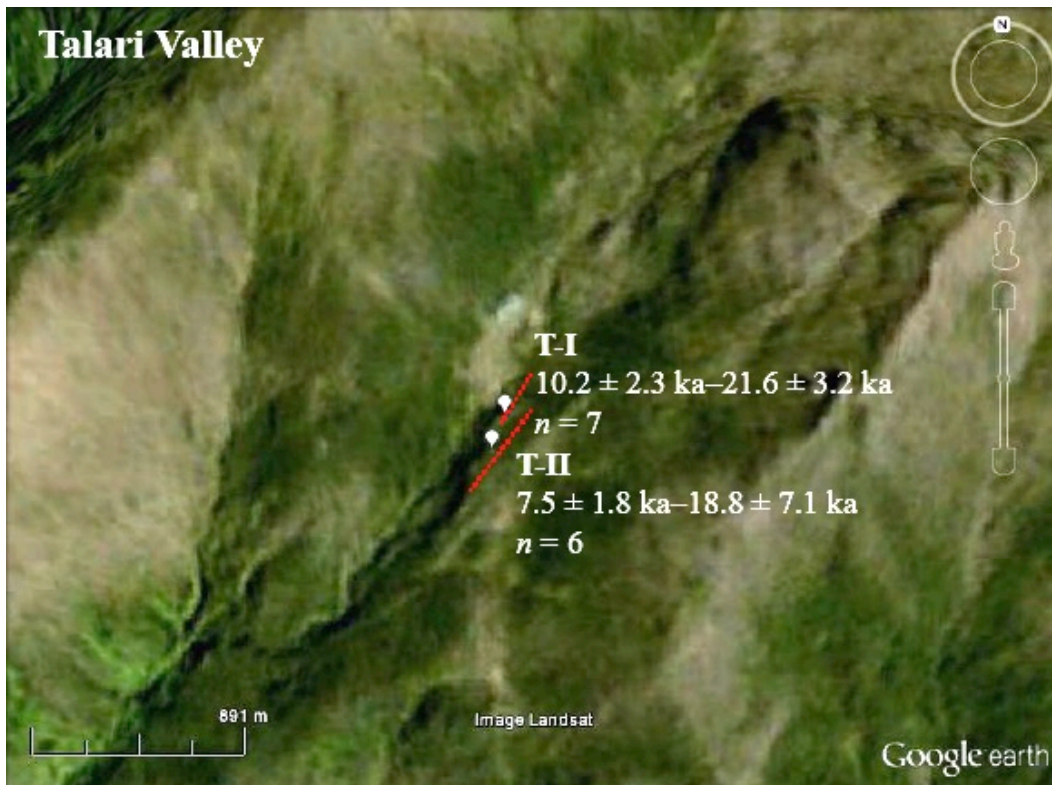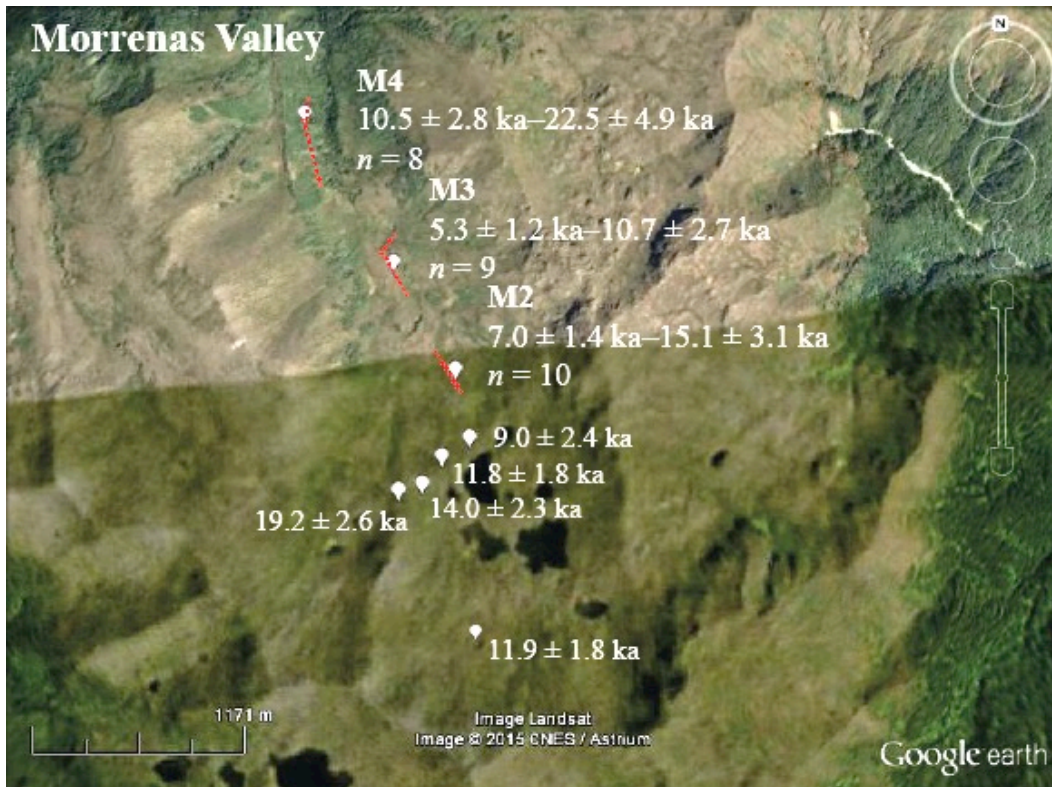
Figure 5: Google Earth images with cosmogenic ^{36}Cl exposure ages from the Morrenas Valley and Talari Valleys. Dashed red lines indicate moraines.

Table 1: Measured ^{36}Cl concentrations and calculated exposure ages from the Morrenas and Talari Valleys using CRONUS (Phillips et al., 2002; Version 1.0; http://web1.ittc.ku.edu:8888/html/latest/cl/). Ages assume zero erosion.

Location	Sample ID	Latitude (°)	Longitude (°)	Elevation (m)	Topographic shielding	^{36}Cl/Cl (x 10^{-15})	^{36}Cl exposure age (ka)
Talari Valley	I–2	9.452	– 83.505	3357	0.9880	388 ± 16	13.6 ± 2.2
	I–3	9.452	– 83.505	3357	0.9880	750 ± 100	41.1 ± 5.9
	I–4	9.452	– 83.505	3357	0.9880	402 ± 17	14.0 ± 2.5
	I–6	9.452	– 83.505	3357	0.9880	278 ± 29	10.2 ± 2.3
	I–7	9.452	– 83.505	3357	0.9880	273 ± 12	12.0 ± 2.0
	I–8	9.452	– 83.505	3357	0.9880	274 ± 11	10.7 ± 1.8
	I–9	9.452	– 83.505	3357	0.9880	259 ± 11	21.6 ± 3.2
	I–10	9.452	– 83.505	3357	0.9880	402 ± 15	13.4 ± 2.6
	II–2	9.453	– 83.505	3349	0.9811	19 ± 3	7.5 ± 1.8
	II–5	9.453	– 83.505	3349	0.9811	715 ± 298	18.8 ± 7.1
	II–6	9.453	– 83.505	3349	0.9811	493 ± 33	14.8 ± 2.3
	II–8	9.453	– 83.505	3349	0.9811	345 ± 13	14.1 ± 2.1
	II–9	9.453	– 83.505	3349	0.9811	373 ± 14	12.7 ± 2.2
	II–10	9.453	– 83.505	3349	0.9811	480 ± 26	12.0 ± 2.0
Morrenas Valley	2–1	9.500	– 83.489	3462	0.9869	334 ± 29	15.1 ± 3.1
	2–2	9.500	– 83.489	3462	0.9869	175 ± 9	7.0 ± 1.4
	2–3	9.500	– 83.489	3462	0.9869	208 ± 11	9.4 ± 2.4
	2–4	9.500	– 83.489	3462	0.9869	207 ± 11	10.6 ± 2.1
	2–5	9.500	– 83.489	3462	0.9869	189 ± 19	10.6 ± 2.2
	2–6	9.500	– 83.489	3462	0.9869	189 ± 8	11.4 ± 2.7
	2–7	9.500	– 83.489	3462	0.9869	179 ± 8	10.7 ± 2.5
	2–8	9.500	– 83.489	3462	0.9869	162 ± 7	9.9 ± 2.6
	2–9	9.500	– 83.489	3462	0.9869	197 ± 10	11.8 ± 2.1
	2–10	9.500	– 83.489	3462	0.9869	142 ± 8	8.4 ± 2.3
	3–1	9.505	– 83.492	3391	0.9751	147 ± 9	9.1 ± 2.6
	3–2	9.505	– 83.492	3391	0.9751	86 ± 10	5.3 ± 1.2
	3–3	9.505	– 83.492	3391	0.9751	156 ± 9	9.1 ± 2.3
	3–5	9.505	– 83.492	3391	0.9751	164 ± 9	10.4 ± 2.8
	3–6	9.505	– 83.492	3391	0.9751	139 ± 8	8.7 ± 2.5
	3–7	9.505	– 83.492	3391	0.9751	141 ± 7	8.8 ± 2.5
	3–8	9.505	– 83.492	3391	0.9751	161 ± 8	10.1 ± 2.7
	3–9	9.505	– 83.492	3391	0.9751	171 ± 9	10.7 ± 2.7
	3–10	9.505	– 83.492	3391	0.9751	152 ± 8	9.7 ± 2.8
	4–1	9.513	– 83.496	3310	0.9753	802 ± 27	48.0 ± 13.0
	4–2	9.513	– 83.496	3310	0.9753	123 ± 4	5.1 ± 1.0
	4–3	9.513	– 83.496	3310	0.9753	234 ± 7	13.7 ± 3.2
	4–4	9.513	– 83.496	3310	0.9753	328 ± 14	22.5 ± 4.9
	4–5	9.513	– 83.496	3310	0.9753	336 ± 13	21.8 ± 4.1
	4–6	9.513	– 83.496	3310	0.9753	219 ± 12	15.6 ± 3.1
	4–7	9.513	– 83.496	3310	0.9753	158 ± 9	10.5 ± 2.8
	4–8	9.513	– 83.496	3310	0.9753	237 ± 9	14.8 ± 2.7
	4–9	9.513	– 83.496	3310	0.9753	271 ± 14	15.4 ± 2.5
	4–10	9.513	– 83.496	3310	0.9753	295 ± 15	18.4 ± 3.3
Morrenas cirque	MOR 98–0	9.488	– 83.488	3551	0.9745	305 ± 15	11.9 ± 1.8
	MOR 98–2	9.497	– 83.488	3482	0.9886	154 ± 6	9.0 ± 2.4
	MOR 98–3	9.496	– 83.490	3513	0.9865	293 ± 9	11.8 ± 1.8
	MOR 98–4	9.495	– 83.490	3558	0.9774	310 ± 25	14.0 ± 2.3
	MOR 98–5	9.495	– 83.491	3590	0.9947	427 ± 11	19.2 ± 2.6
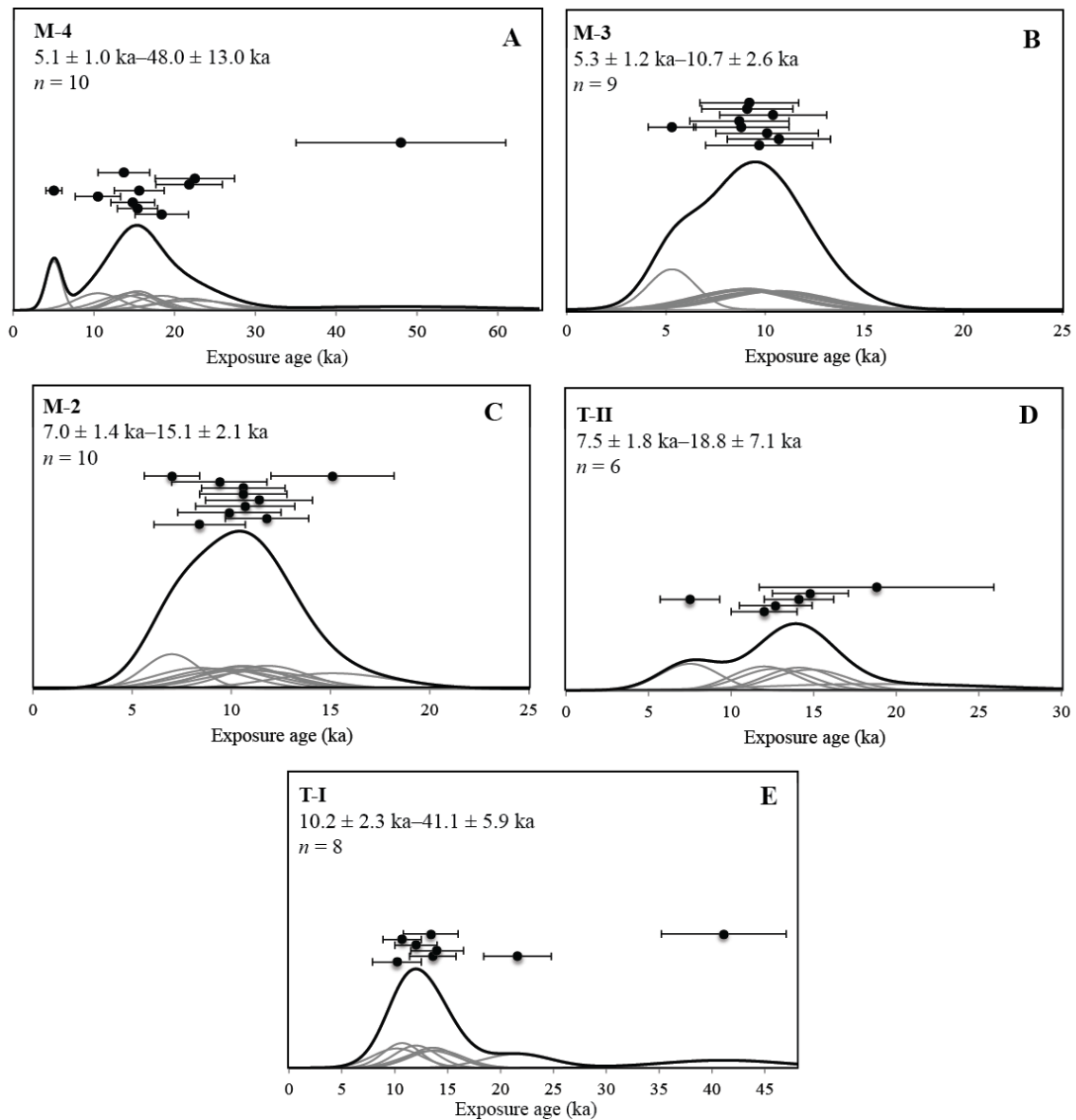
Figure 6: Probability density curves of exposure ages from moraines in the Morrenas and Talari Valleys. Moraines in the Morrenas Valley include: (A) the M4 moraine – associated with the oldest and most extensive moraine complex in the Morrenas Valley, (B) the M3 moraine up-valley from the M4 moraine, and (C) the M2 moraine farther up-valley from the M3 moraine. Moraines in the Talari Valley include: (D) the T-II moraine, and (E) the T-I moraine.

30

moraine at an elevation of 3391 m. Ages range from 10.7 ± 2.7 to 5.3 ± 1.2 ka (n = 9).

The PDF of M3 ages (Figure 6B) shows that ages cluster around 9.1 ka. The Chirripó II

(M2) moraine complex is ~0.8 km up-valley from the Chirripó III (M3) moraine and ~1.6

km up-valley from Chirripó IV (M4). Boulders were sampled atop this moraine at an

elevation of 3462 m. Ages range from 15.1 ± 3.1 to 7.0 ± 1.4 ka (n = 10). The PDF of M2

ages (Figure 6C) indicates that ages cluster around 10.5 ka. The Chirripó I (MOR)

moraine complex is closest to the Chirripó headwall, and at an elevation of ~3550 m.

This complex corresponds to several moraines that surround glacial lakes within the

cirque. Within this complex, four ages from these moraines range from 14.0 ± 2.3 to 9.0

± 2.4 ka. A lateral moraine is present on the eastern wall of the cirque. The exposure age

from this moraine is 19.2 ± 2.6 ka, and most likely corresponds to the older and most

extensive Chirripó IV moraine complex. I did not plot MOR ages as a PDF because it

would not be accurate to analyze cluster or outliers of five separate moraines in a single

PDF.

5.2 Talari Valley

Fifteen cosmogenic ^{36}Cl exposure ages from two moraines constrain the timing of

glacial events in the Talari Valley. Ages from the T-II moraine, at an elevation of 3349 m

range from 18.8 ± 7.1 to 7.5 ± 1.8 ka (n = 6). The PDF of T-II ages (Figure 6D) shows

ages cluster around 13.3 ka. The T-I moraine is ~0.1 km up-valley from the T-II moraine,

and at an elevation of 3357 m. Ages from the T-I moraine range from 41.1 ± 5.9 to 10.2 ±

2.3 (n =8). The PDF of T-I ages (Figure 6E) indicates ages cluster around 12.3 ka.

5.3 Uncertainties caused by scaling models

Scaling factors describe the variability of the cosmic-ray flux and the influence of the magnetic fields of Earth and the Sun (Dunai, 2010). Different scaling models have been introduced to determine the site-specific nuclide production rate based on the reference production rates from sea level and high latitude (Dunai, 2010). The CRONUS-Earth ^{36}Cl Exposure Age Calculator (Phillips et al., 2002) provides two scaling models: Desilets and Zreda (Desilets and Zreda, 2003; Desilets et al., 2006) and Lifton and Sato (Lifton et al., 2008; Sato et al., 2008; Lifton et al., 2014). The difference between these two models is that the Desilets and Zreda model used neutron monitors to measure nucleon fluxes and incorporates a time-dependent geomagnetic field (Lifton et al., 2014), whereas the Lifton and Sato model is time-independent and incorporates variability of solar and atmospheric cosmic-ray intensities.

I used both scaling models to examine the variability of calculated exposure ages, assuming all other variables to be the same (a complete table of the results is provided in Appendix B). Results indicated that exposure ages increased an average of ~1.7 ka using the Lifton and Sato scaling model (Lifton et al., 2008; Sato et al., 2008; Lifton et al., 2014). I also calculated the percent change of exposure ages between the two models (Figure 7). Percent changes range from 3.20–19.05% with an average value of 13.99%. The negative trend in Figure 7 indicates that the younger exposure ages have a greater percent change between the scaling models. To assess which model is more suitable for this study, I compared radiocarbon ages (*n* = 5) from basal sediments of glacial lakes within the Morrenas cirque (Orvis and Horn, 2000; Lane et al., 2011) to the ^{36}Cl exposure ages within the Morrenas cirque (*n* = 4; MOR) (Table 2; Figure 8). S. Horn calibrated the
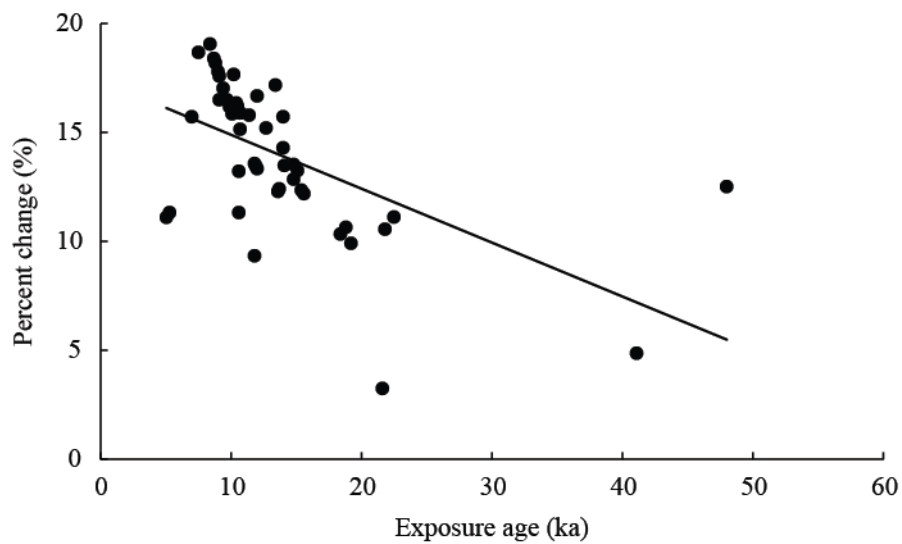
Figure 7: Percent change (%) between [36]Cl exposure ages calculated using the Desilets and Zreda scaling model (Desilets and Zreda, 2003; Desilets et al., 2006) and the Lifton and Sato scaling model (Lifton et al., 2008; Sato et al., 2008; Lifton et al., 2014).

radiocarbon dates using Calib 7.0.2 (Stuiver and Reimer, 1993) and the dataset of Reimer et al. (2013). The comparison suggests that the Desilets and Zreda scaling model is a better overall match with the radiocarbon ages, but the comparison is not straightforward as radiocarbon ages on basal organics in lake basins formed by moraines are expected to be somewhat younger than the ages of the moraines, but just how much younger they might be is uncertain. Most of the basal ages are younger than the cosmogenic ages determined with both scaling models, but one age using the Desilets and Zreda scaling model is younger than the basal ages, which appears unlikely.

One potential reason why the Desilets and Zreda scaling model yielded cosmogenic ages closer to the radiocarbon ages on basal lake sediments is that the Lifton and Sato scaling model integrates the influence of solar modulation on the neutron monitor intensities that is more important at high latitudes (Lifton et al., 2008; Sato et al., 2008; Lifton et al., 2014), whereas the Desilets and Zreda scaling model (Desilets and Zreda, 2003; Desilets et al., 2006) was developed at low-latitude locations (Hawaii and Bangalore), and may be more suitable to the low latitude of Costa Rica.

5.4 Uncertainties caused by boulder surface erosion

Boulder surface erosion can cause uncertainties in surface exposure ages. For cosmogenic ^{10}Be and ^{26}Al, production rate exponentially declines with increasing depth below the surface (Lal and Peters, 1967; Liu et al., 1994); thus, surface erosion tends to reduce the surface production rate, yielding an apparently younger exposure age. The nuclide production-depth relationship for ^{36}Cl is relatively complicated due to the ^{36}Cl

Table 2: Basal radiocarbon dates (ka cal BP) from glacial lakes 0A, 1, and 4 within the Morrenas cirque (Horn, 1990; Orvis and Horn, 2000; Lane et al., 2011) and cosmogenic [36]Cl exposure ages (ka) from within the Morrenas cirque.

Publication	Sample ID	Age	Calibrated age 2-sigma range (ka BP)	Area under curve
Orvis & Horn	0A	8.670±0.06	9.797 – 9.531	0.9697
			9.817 – 9.803	0.0097
			9.866 – 9.847	0.0134
			9.885 – 9.876	0.0072
Lane et al. 2011	1 (core 1)	9.811±0.05	11.315 – 11.167	1.0000
Horn 1990	1 (core 2)	8.900±0.10	10.235 – 9.679	1.0000
Horn 1990	1 (core 2)	10.140±0.12	12.165 – 11.267	0.9908
			12.230 – 12.210	0.0057
			12.368 – 12.355	0.0035
Orvis & Horn	4	8.580±0.07	9.704 – 9.457	0.9962
			9.729 – 9.723	0.0038
This study	MOR 98–0	11.9 ± 1.7		
This study	MOR 98–2	9.0 ± 2.4		
This study	MOR 98–3	11.8 ± 1.8		
This study	MOR 98–4	14.0 ± 2.3		
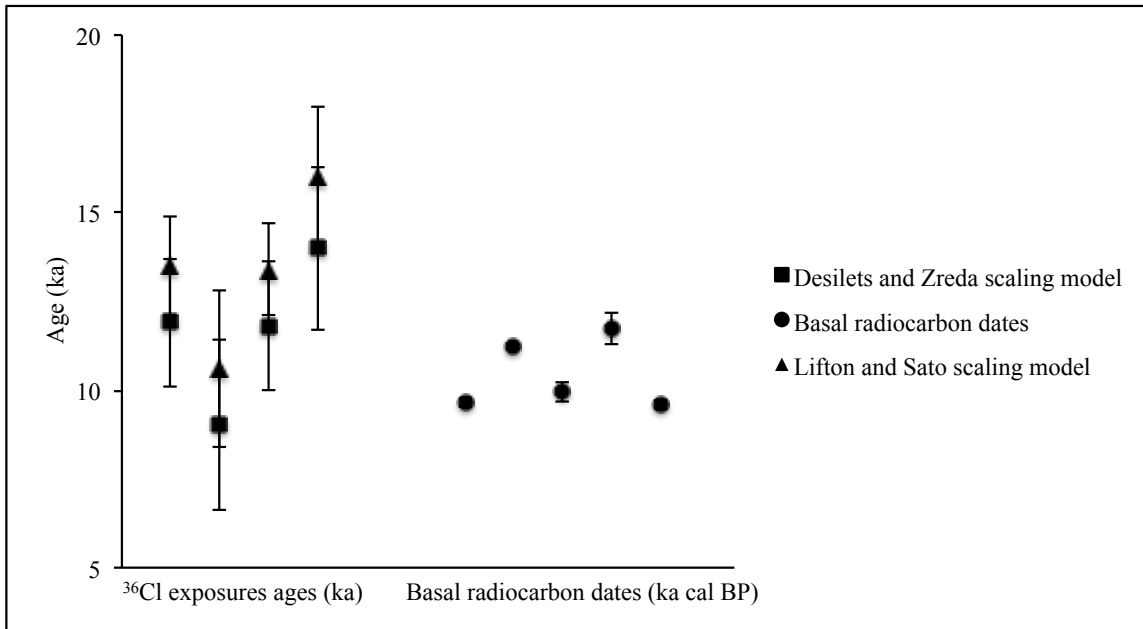
Figure 8: Cosmogenic [36]Cl exposure ages using the Desilets and Zreda scaling model and the Lifton and Saton scaling model from moraines within the Morrenas cirque compared to radiocarbon dates from glacial lake sediments within the Morrenas cirque (Horn, 1990; Orvis and Horn, 2000; Desilets and Zreda, 2003; Desilets et al., 2006; Lifton et al., 2008; Sato et al., 2008; Lane et al., 2011; Lifton et al., 2014). Basal radiocarbon dates are the weighted mean of the probability distribution (calculated by Horn from files output by Calib 7.0.2). Cosmogenic ages represent a single age from a single moraine. Error bars are the 2-sigma ranges.

production from the neutron-absorption of ^{35}Cl near the surface (Gosse and Phillips, 2001). The ^{36}Cl production rate would increase within the top 15–20 cm of the rock surface and then decrease with increasing depth (Gosse and Phillips, 2001). Therefore, a smaller erosion rate may result in an apparently older ^{36}Cl exposure age.

I tested the effect of boulder surface erosion by calculating exposure ages using different erosion rates. To keep all other inputs the same, I calculated the exposure ages for surface erosion rates of 0 mm/kyr, 1 mm/kyr, 2 mm/kyr, and 3 mm/kyr, respectively (a complete table of the results is provided in Appendix B). I then calculated the percent change between 0 mm/kyr–1 mm/kyr, 0 mm/kyr–2 mm/kyr, and 0 mm/kyr–3 mm/kyr (Figure 9). The average percent changes are 0.66%, 1.31%, and 1.75% between the ages derived using 0 mm/kyr and those derived using 1 mm/kyr, 2 mm/kyr, and 3 mm/kyr, respectively. Positive trends exist between the age differences and exposure ages in all three comparisons. The highest average percent change is between 0 mm/kyr and 3 mm/kyr, indicating increased age differences for higher erosion rate disparity.
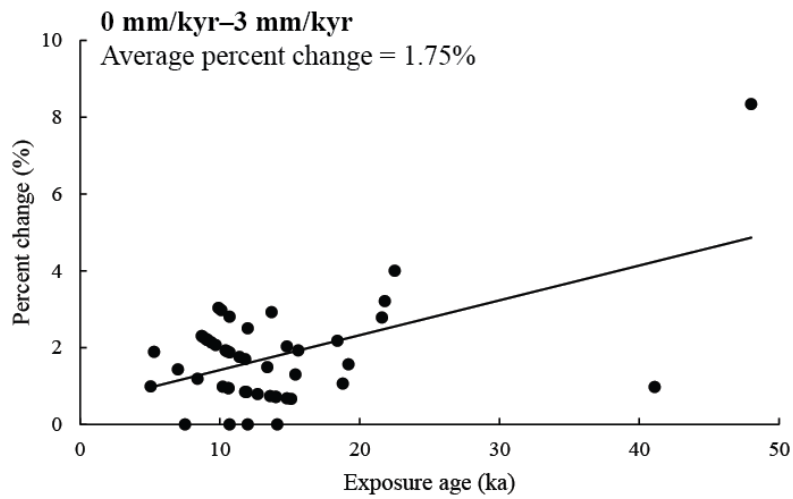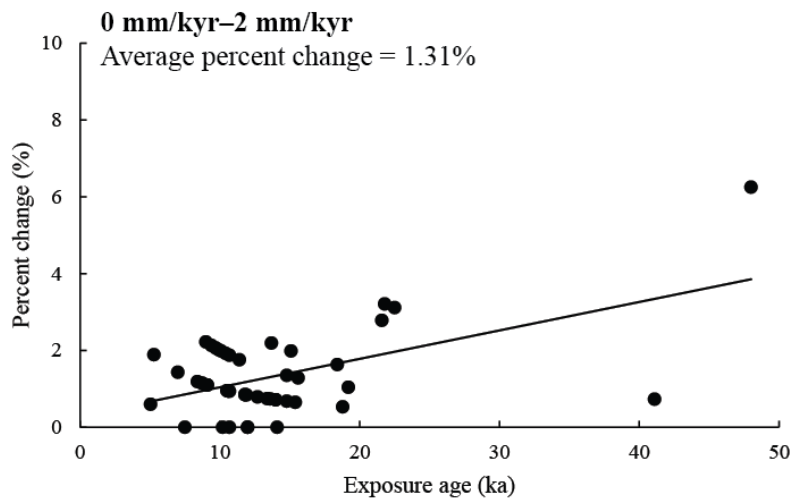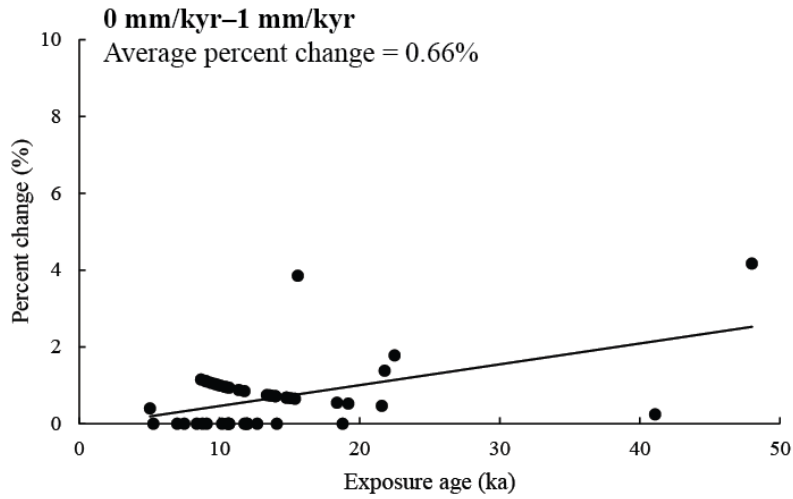
Figure 9: Scatter plot showing percent change of cosmogenic [36]Cl exposure ages (ka) as erosion rate (mm/kyr) increases.

CHAPTER 6

Discussion

6.1 Glacial chronology

Cosmogenic ^{36}Cl exposure ages from the Morrenas and Talari Valleys indicate a glacial advance ~22–18 ka extending 3.2 km and 3.4 km down valley, respectively. This glacial event was broadly synchronous with the timing of the global LGM (28–16 ka; Glasser et al., 2011). Oxygen isotope records show a sharp decrease in temperature during the LGM (Figure 10). Paleo-sea surface temperature (SST) estimates suggest that low altitude land temperatures in the Neotropics (Mexico, Central America, and the Northern Andes) were on average 5–6 °C lower than today during the LGM (Farrera et al., 1999; Mark et al., 2005). This temperature depression was sufficient to drive glacial advances in the highlands of Costa Rica and other regions in the Neotropics (Mexico, Vazquez-Selem and Heine, 2004; Venezuela, Carcaillet et al., 2013).

Following LGM advance, exposure ages indicate periods of retreat and standstills throughout the Lateglacial and early Holocene in the Morrenas and Talari Valleys. Oxygen isotope records indicate a global post-LGM warming trend that has continued through the Holocene (Figure 10). However, this overall warming has been periodically interrupted by cooler phases. Post-LGM moraine formation most likely occurred during these short cooling periods causing glacial standstills. Retreat most likely commenced when warmer phases returned. It appears that the exposure ages from the Chirripó II (M2) and Chirripó III (M3) moraines cluster around the Younger Dryas stadial. However, given the large uncertainty in these exposure ages, I am not confident to argue the

39
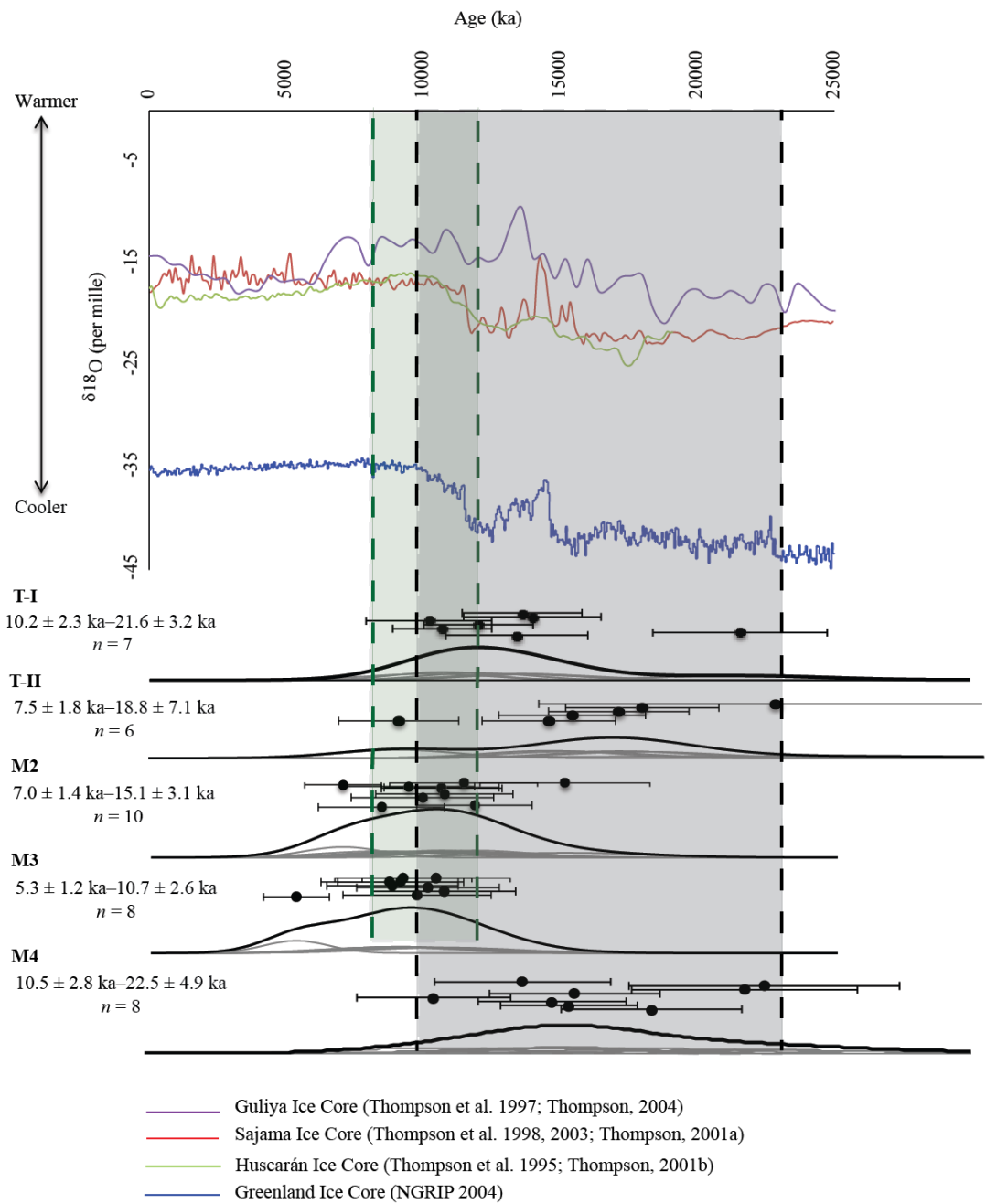
Figure 10: Oxygen isotope and probability density curves of exposure ages of moraines in the Morrenas and Talari Valleys. Age ranges exclude outliers.

occurrence of glacial advance in the Morrenas and Talari Valleys during the Younger Dryas. In the Morrenas cirque, the lack of ages younger than ~9 ka suggests no glacial advances post ~9 ka. These results are similar to the results obtained from radiocarbon ages of lake sediments within the Morrenas cirque (Table 2; Figure 8). No exposure ages from moraines within the Talari cirque were dated, and the absence of glacial lakes within the cirque prevents radiocarbon dating of lake sediments. Because of similar glacial extent and exposure ages in both the Morrenas and Talari Valleys, it can be inferred that complete deglaciation in the Talari Valley occurred during a period similar to the Morrenas Valley.

The elevation vs. age plot (Figure 11) shows similarities in the timing and extent of glacial events between the Morrenas and Talari Valleys. Specifically, the age of the M4 moraine (Morrenas Valley) is correlated with the ages of the T-I and T-II moraines (Talari Valley). In the Morrenas Valley, the oldest and most extensive moraine (M4) lies at an elevation of 3310 m. Excluding outliers, ages from this moraine range from 22.5–10.5 ka and ages from the T-II moraine (3349 m a.s.l.) range from 18.8–7.5 ka. The T-I moraine is only ~0.1 km up-valley from the T-II moraine at 3357 m a.s.l. with an age range of 21.6–10.2 ka. Similar exposure ages, geomorphic evidence, and the close proximity of these two Talari moraines suggest that they were most likely formed during the same glacial stage. The comparable age ranges and elevations between the M4, T-I, and T-II moraines suggest similar timing and extent of glacial advances in both valleys during the LGM.
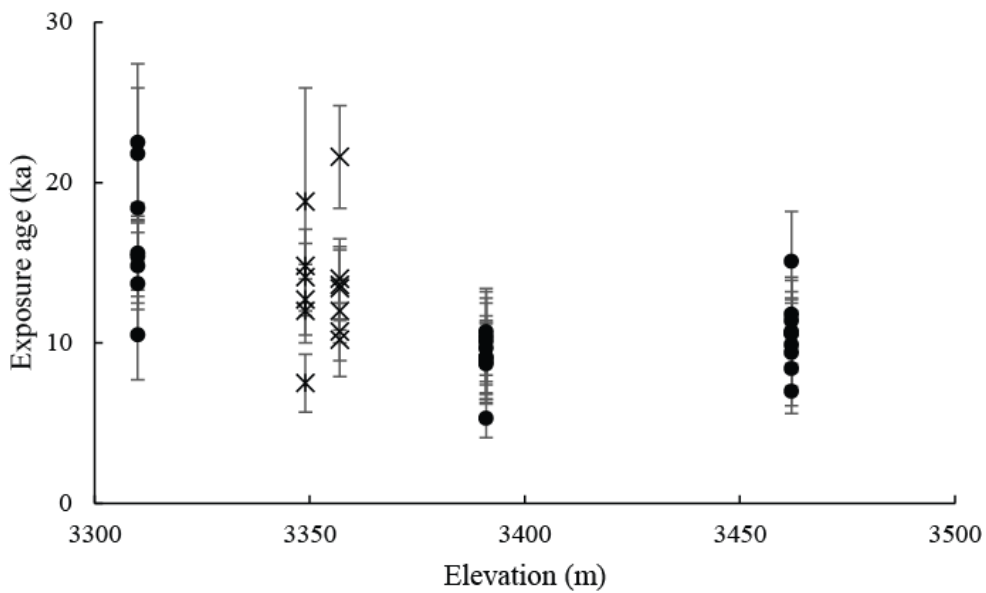
Figure 11: Elevation (m) vs. age (ka) plot for moraines in the Morrenas and Talari Valleys. Black dots represent exposure ages from moraines complexes within the Morrenas Valley. Black "x" marks represent exposure ages from moraine complexes within the Talari Valley.

6.2 Paleoclimate interpretations

Orvis and Horn (2000) reconstructed ELAs in the Morrenas Valley. They determined the ELA to be 3355 m for the most extensive moraine complex, Chirripó IV (M4), in the Morrenas Valley (Orvis and Horn, 2000). Lachinet and Selzter (2002) also mapped and reconstructed ELAs of three moraine complexes in the Morrenas and Talari Valley (Table 3). They defined the most extensive moraine complex as Talamanca, which exists in both valleys (Lachinet and Seltzer, 2002). They determined the Talamanca ELA to be 3532 m in the Talari Valley and 3502 m in the Morrenas Valley (Lachinet and Seltzer, 2002).

Orvis and Horn (2000) suggested that the Chirripó IV (M4) moraine complex might have formed during a time when climate was simultaneously colder and wetter, in comparison to the climate during the formation of moraine complexes upvalley thought to be associated with MIS 2 and possibly MIS 4. The new exposure ages indicate that the Chirripó IV (M4) moraine complex was formed during the LGM (early part of MIS 2), and that moraines upvalley formed during standstills or brief advances during the Lateglacial. Paleoclimate records show that climate was colder and drier in the tropics during MIS 2 compared to MIS 4 (Schubert, 1988; Thouret et al., 1996; Orvis and Horn, 2000). With the new cosmogenic dates, however, the appropriate comparison is between the LGM and postglacial climates on the massif. Chirripó IV moraines certainly formed under conditions that were colder—and potentially also wetter—than conditions during the standstills or small advances that formed the Chirripó III and II moraine complexes.

Lachinet and Seltzer (2002) discussed evidence of steeper temperature depression

Table 3: ELA reconstructions of the Morrenas and Talari Valleys (Orvis and Horn, 2000; Lachinet and Seltzer, 2002). See Orvis and Horn (2000) for additional ELA reconstructions using other methods.

Publication	Method	Valley	Advance	ELA (m)
Lachinet and Seltzer (2002)	THAR = AAR = 0.7	Talari	Talamanca	3532
			Chirripó	3580
			Talari	3586
		Morrenas	Talamanca	3502
			Chirripó	3583
			Talari	3616
Orvis and Horn (2000)	BR = 25	Morrenas	Chirripó IV	3355
			Chirripó III	3470
			Chirripó II	3484

at higher altitudes in the tropics. In contrast to the evidence indicating that Pacific SSTs in the tropics only reduced 2–3 °C during LGM (Lee and Slowey, 1999; Lea et al., 2000; Pigati et al., 2008), reconstructed tropical ELA depressions indicate cooling at higher altitudes more than twice that estimated for Pacific SSTs (Crowley, 2000; Mark et al., 2005; Pigati et al., 2008). Orvis and Horn (2000) used their ELA reconstructions to determine temperature depressions for each moraine complex in the Morrenas Valley. They calculated temperature depressions of −7.36 ± 0.02 °C for Chirripó I (MOR), −7.51 ± 0.05 °C for Chirripó II (M2), −7.45 ± 0.06 °C for Chirripó III (M3), and −7.79 ± 0.25 °C for Chirripó IV (M4) (Orvis and Horn, 2000). These reconstructions indicate more than 7 °C temperature depressions during the LGM and subsequent Lateglacial and early Holocene periods in the Morrenas and Talari Valleys.

6.3 Comparison with other regions in Tropical America

The cosmogenic ^{36}Cl glacial chronology indicates a LGM glacial event during 22–18 ka in the Morrenas and Talari Valleys. The timing of this LGM event is broadly synchronous with the global LGM (28–16 ka; Glasser et al., 2011). This indicates that the timing of glacial events in the Cordillera de Talamanca was broadly synchronous with the timing of glacial events at mid- to high latitudes. Previously established cosmogenic glacial chronologies help determine synchronous or asynchronous timing of LGM events in tropical America. The glacial chronology of the Cordillera de Talamanca can be compared with these existing chronologies.

LGM

Recent climate reconstructions have suggested a global mean temperature depression of 4.0 ± 0.8 °C during the LGM (Annan and Hargreaves, 2013). Exposure ages presented in this study indicate that maximum glacial extent occurred in both the Morrenas and Talari Valleys during this period. Many glacial chronologies provide evidence of LGM glacier events in the tropics and subtropics (Kaplan et al., 2007; Kaplan et al., 2008; Kull et al., 2008; Bromley et al., 2009; Hein et al., 2009; Zech et al., 2009; Hein et al., 2010; Glasser et al., 2011; Wesnousky et al., 2012; Carcaillet et al., 2013). These LGM advances were broadly synchronous with LGM advances at mid- to high latitudes in North America (Briner et al., 2005; Briner and Kaufman, 2008; Licciardi and Pierce, 2008; Phillips et al., 2009; Young et al., 2009; Rood et al., 2011; Young et al., 2011; Laabs et al., 2013).

Lateglacial and early Holocene

Multi-proxy evidence, including isotopic records from ice cores and [10]Be exposure ages, indicate synchronous retreat of LGM glaciers in both hemispheres (e.g., Schaefer et al., 2006). Post-LGM warming was punctuated with short cooling periods throughout the Lateglacial and early Holocene, which likely stalled retreat or caused glaciers to re-advance. Exposure ages presented in this study indicate periods of advance, standstill, or retreat during the Lateglacial and early Holocene. Previously published chronologies in the tropics and subtropics have also indicated comparable Lateglacial and early Holocene events (Vazquez-Selem and Heine, 2004; Farber et al., 2005; Zech et al., 2006; Pigati et al., 2008; Hall et al., 2009; Bromley et al., 2009; Smith et al., 2009; Zech

46

et al., 2009; Kaplan et al., 2011; Carcaillet et al., 2013; Jomelli et al., 2014), similar to Lateglacial and early Holocene events widely reported in higher latitudes (e.g., Briner et al., 2002; Owen et al., 2003; Balco et al., 2009). This study contributes to the growing literature of chronologies in the tropics, strengthening the argument that the timing of LGM and Lateglacial/early Holocene events between North and South America was broadly synchronous.

Pre-LGM

Glacial events have also been dated to MIS 3 or older in tropical regions of Central and South America. In Mexico, there are exposure ages of moraines dated to ~195 ka, and most likely represent the most extensive glacial event (Vazquez-Selem and Heine, 2004). In the Andes, moraines have been dated from MIS 4 to as old, or older than, MIS 13 (Smith et al., 2002; Farber et al., 2005; Smith et al., 2005; Kull et al., 2008; Smith et al., 2008; Zech et al., 2008; Hein et al., 2009; Hein et al., 2010; Glasser et al., 2011). In these regions, younger MIS 2 advances did not override older moraines, indicating that older advances were more extensive than LGM advances (Farber et al., 2005; Glasser et al., 2011).

Exposure ages presented in this study do not indicate the occurrence of glacier events before MIS 2 in Costa Rica. Compared to the high Andes, precipitation is higher in Costa Rica. For example, climate data from the Cerro Páramo meteorological station (3466 m; 9°33'41" N, 83°45'18" W), located ~30 km west of Cerro Chirripó, recorded a mean annual precipitation of 2581 mm (Lane et al., 2011). Post-glacial fluvial processes could have eroded moraines older than MIS 2. It is also possible that glacial events older

than MIS 2 occurred in the Morrenas and Talari Valleys, but were less extensive than the LGM event. Therefore, subsequent LGM advances would have overridden these older moraines. Another possibility is that no glacier events occurred in the Morrenas and Talari Valleys prior to the LGM. Further studies are necessary to investigate these different possibilities.

Younger Dryas and Holocene glacial events

Cosmogenic exposure ages have indicated Younger Dryas and Holocene glacial events in the Andes (Douglass et al., 2005; Zech et al., 2006; Bromley et al., 2009; Glasser et al., 2009; Smith et al., 2009). Exposure ages presented in this study are scattered with relatively large uncertainty, so they cannot be used to confirm the Younger Dryas event. However, radiocarbon ages from glacial lake sediments of the Morrenas Valley indicate post-Younger Dryas deglaciation, suggesting a possible glacial standstill or small advance during the Younger Dryas (Orvis and Horn, 2000).

Exposure ages in this study indicate no glacier events post ~9 ka in both the Morrenas and Talari Valleys. These results are consistent with the lack of evidence of glacial advances in lake sediments in the Morrenas cirque, and with radiocarbon ages, which indicated complete deglaciation after 12.4 ka cal BP and before 9.7 ka cal BP in the Morrenas Valley (Orvis and Horn, 2000, and S. Horn, pers. comm.). Similar results also indicated complete glacial retreat ~9 ka in Venezuela (~8.8 °N) (Carcaillet et al., 2013), which has similar latitudes to the Cordillera de Talamanca (9.29 °N).

CHAPTER 7

Conclusions

The major findings of this research are summarized below:

1) cosmogenic ^{36}Cl exposure ages indicate a LGM glacial event ~22–18 ka in the Morrenas and Talari Valleys, which is synchronous with the global LGM;

2) exposure ages indicate periods of glacial retreat, standstill, or minor advance through the Lateglacial and early Holocene ~18–10 ka;

3) elevation and age comparison suggests similar timing and extent of glacial advances in the Morrenas and Talari Valleys;

4) comparisons between the ^{36}Cl exposure ages calculated using different scaling models and the radiocarbon ages from glacial lake sediments suggest that the Desilets and Zreda scaling model may be more suitable for this study; and

5) minor variations (<5%) between exposure ages derived using zero and 3 mm/kyr erosion rate (a possible maximum erosion rate) indicate that surface erosion is probably not a significant factor affecting the exposure ages of this study.

The cosmogenic ^{36}Cl exposure ages expand the previous glacial chronology determined using radiocarbon ages from glacial lake sediments in the Morrenas Valley (Orvis and Horn, 2000). In particular, the exposure ages suggest a major LGM glacial event before (~22–18 ka) in the Morrenas and Talari Valleys, followed by periods of standstill and retreat during the Lateglacial and early Holocene. This glacial event in the tropics is synchronous with the global LGM. Although evidence of Younger Dryas

glacial advances exists around the world, exposure ages still could not confirm the occurrence of a Younger Dryas glacial event in this study area due to the large uncertainty. Radiocarbon ages of lake sediment cores from the Morrenas Valley indicated complete deglaciation after 12.4 ka cal BP but before 9.7 ka cal BP (Orvis and Horn, 2000). Lack of exposure ages younger than ~9 ka suggests this LGM event and subsequent deglaciation during the Lateglacial and early Holocene were the most recent glacial events in the Morrenas and Talari Valleys.

Studies suggested that low altitude land temperatures in the Neotropics (Mexico, Central America, and the Northern Andes) were on average 5–6 °C lower than today during the LGM (Farrera et al., 1999; Mark et al., 2005). Orvis and Horn (2000) estimated a temperature depression of -7.79 ± 0.25 °C during the Chirripó IV moraine formation, corresponding to the LGM event in the Morrenas and Talari Valleys. Temperatures were cold enough to drive glacier advance ~3.2 km down-valley during the LGM.

Future work will develop a ~26 m DEM using a paper-based topographic map of the study site. This DEM will enable the research team to conduct an accurate terrain analysis and develop a glacier simulation model. I am currently working on developing a large dataset containing exposure ages and necessary information from previously published cosmogenic chronologies in North, Central, and South America. Although uncertainties exist, cosmogenic nuclide exposure dating is a key method for establishing glacial chronologies, and improving the understanding of glacial patterns in the tropics. Further research will help determine if the timing of glacial events in the tropics was

broadly synchronous or asynchronous with the timing of glacial events in mid-to high

latitudes.

REFERENCES

Annan, J.D., Hargreaves, J.C., 2013. A new global reconstruction of temperature changes at the Last Glacial Maximum. Clim. Past 9, 367–376.

Applegate, P.J., Urban, N.M., Keller, K., Lowell, T.V., Laabs, B.J.C., Kelly, M.A., Alley, R.B., 2012. Improved moraine age interpretations through explicit matching of geomorphic process models to cosmogenic nuclide measurements from single landforms. Quaternary Res. 77, 293–304.

Balco, G., Briner, J., Finkel, R.C., Rayburn, J.A., Ridge, J.C., Schaefer, J.M., 2009. Regional beryllium-10 production rate calibration for late-glacial northeastern North America. Quat. Geochronol. 4, 93–107.

Balco, G., 2011. Contributions and unrealized potential contributions of cosmogenic-nuclide exposure dating to glacier chronology, 1990–2010. Quaternary Sci. Rev. 30, 3–27.

Ballantyne, A.P., Lavine, M., Crowley, T.J., Liu, J., Baker, P.B., 2005. Meta-analysis of tropical surface temperatures during the Last Glacial Maximum. Geophys. Res. Lett. 32, L05712.

Barquero, J., Ellenberg, L., 1983. Geomorfologia del Piso Alpino del Chirripó en La Cordillera de Talamanca, Costa Rica. Revista Geográfica de América Central 17–18, 293–299.

Barquero, J., Ellenberg, L., 1986. Geomorphologie der alpinen Stufe des Chirripó in Costa Rica. Eiszeitalter u. Gegenwart 36, 1–9.

Benn, D.I., Owen, L.A., Osmaston, H.A., Seltzer, G.O., Porter, S.C., Mark, B., 2005. Reconstruction of equilibrium-line altitudes for tropical and subtropical glaciers. Quatern. Int. 138–139, 8–21.

Bergoeing, J.P., 1977. Modelado glacier en la Cordillera de Talamanca. Informe

    Semestral julio-diciembre 1977 Instituto Geográfico Nacional, San José, Costa

    Rica.

Briner, J.P., Kaufman, D.S., Werner, A., Caffee, M., Levy, L., Manley, W.F., Kaplan,

    M.R., Finkel, R.C., 2002. Glacier readvance during the late glacial (Younger

    Dryas?) in the Ahklun Mountains, southwestern Alaska. Geology 30, 679–682.

Briner, J.P., Kaufman, D.S., Manley, W.F., Finkel, R.C., Caffee, M.W., 2005.

    Cosmogenic exposure dating of late Pleistocene moraine stabilization in Alaska.

    Geol. Soc. Am. Bull. 117, 1108–1120.

Briner, J.P., Kaufman, D.S., 2008. Late Pleistocene mountain glaciation in Alaska: key

    chronologies. J. Quaternary Sci. 23, 659–670.

Bromley, G.R.M., Schaefer, J.M., Winckler, G., Hall, B.L., Todd, C.E., Rademaker,

    K.M., 2009. Relative timing of last glacial maximum and late-glacial events in the

    central tropical Andes. Quaternary Sci. Rev. 28, 514–526.

Bush, M.B., Correametrio, A.Y., Hodell, D.A., Brenner, M., Anselmetti, F.S., Ariztegui,

    D., Mueller, A.D., Curtis, J.H., Grzesik, D.A., Burton, C., Gilli, A., 2009. Re-

    evaluation of climate change in lowland Central America during the last glacial

    maximum using new sediment cores from Lake Peten Itza, Guatemala. Dev.

    Paleoenviron. Res. 14, 113–128.

Caffrey, M.A., Taylor, M.J., Sullivan, D.G., 2011. A 12,000-year record of vegetation

    and climate change from the Sierra De Los Cuchumatanes, Guatemala. J. Lat. Am.

    Geogr. 10, 129–151.

Carcaillet, J., Angel, I., Carrillo, E., Audemard, F.A., Beck, C., 2013. Timing of the last deglaciation in the Sierra Nevada of the Merida Andes, Venezuela. Quaternary Res. 80, 482–494.

Chen, Y., Li, Y., Wang, Y., Zhang, M., Cui, Z., Yi, C., Liu, G., 2015. Late Quaternary glacial history of the Karlik Range, easternmost Tian Shan, derived from [10]Be surface exposure and optically stimulated luminescence datings. Quaternary Sci. Rev. 115, 17–27.

CLIMAP, 1981. Seasonal reconstructions of the Earth's surface at the last glacial maximum. Geological Society of America Map and Chart Series: MC–36, Geological Society of America.

Crowley, T.J., 2000. CLIMAP SSTs re-revisited. Clim. Dynam. 16, 241–255.

Davis, R.Jr., Schaeffer, O.A., 1955. Chlorine-36 in nature. Ann. N. Y. Acad. Sci. 62, 105–122.

Delgado, H., 1997. The glaciers of Popocatépetl Volcano (Mexico): Changes and causes. Quatern. Int. 43–44, 53–60.

Desilets, D., Zreda, M., 2003. Spatial and temporal distribution of secondary cosmic-ray nucleon intensities and applications to in situ cosmogenic dating. Earth Planet. Sc. Lett. 206, 21–42.

Desilets, D., Zreda, M., Prabu, T., 2006. Extended scaling factors for in situ cosmogenic nuclides: New measurements at low latitude. Earth Planet. Sci. Lett. 246, 265.

Douglass, D.C., Singer, B.S., Kaplan, M.R., Ackert, R.P., Mickelson, D.M., Caffee, M.W., 2005. Evidence of early Holocene glacial advances in southern South America from cosmogenic surface-exposure dating. Geology 33, 237–240.

Dunai, T. J., 2010. Cosmogenic Nuclides: Principles, Concepts and Applications in the Earth Surface Sciences. Cambridge, UK: Cambridge University Press.

Farber, D.L., Hancock, G.S., Finkel, R.C., Rodbell, D.T., 2005. The age and extent of tropical alpine glaciation in the Cordillera Blanca, Peru. J. Quaternary Sci. 20, 759–776.

Farrera, I., Harrison, S.P., Prentice, I.C., Ramstein, G., Guiot, J., Bartlein, P.J., Bonnefille, R., Bush, M., Cramer, W., von Grafenstein, U., Holmgren, K., Hooghiemstra, H., Hope, G., Jolly, D., Lauritzen, S-E., Ono, Y., Pinot, S., Stute, M., Yu, G., 1999. Tropical climates at the Last Glacial Maximum: a new synthesis of terrestrial palaeoclimate data. I. Vegetation, lake-levels and geochemistry. Clim. Dynam. 15, 823–856.

Glasser, N.F., Clemmens, S., Schnabel, C., Fenton, C.R., McHargue, L., 2009. Tropical glacier fluctuations in the Cordillera Blanca, Peru between 12.5 and 7.6 ka from cosmogenic [10]Be Dating. Quaternary Sci. Rev. 28, 3448–3458.

Glasser, N.F., Jansson, K.N., Goodfellow, B.W., Angelis, H., Rodnight, H., Rood, D.H., 2011. Cosmogenic nuclide exposure ages for moraines in the Lago San Martin Valley, Argentina. Quaternary Res. 75, 636–646.

Gosse, J.C., Phillips, F.M., 2001. Terrestrial in situ cosmogenic nuclides: theory and application. Quaternary Sci. Rev. 20, 1475–1560.

Hall, S.R, Farber, D.L., Ramage, J.M., Rodbell, D.T., Finkel, R.C., Smith, J.A., Mark, B.G., Kassel, C., 2009. Geochronology of Quaternary glaciations from the Tropical Cordillera Huayhuash, Peru. Quaternary Sci. Rev. 28, 2991–3009.

Hastenrath, S., 1973. On the Pleistocene glaciation of the Cordillera de Talamanca, Costa
Rica. Zeitschrift für Gletscherkunde und Glazialgeologie. 9, 105–121.

Hastenrath, S., 2009. Past glaciation in the tropics. Quaternary Sci. Rev. 29, 790–798.

Hein, A.S., Hulton, N.R.J., Dunai, T.J., Schnabel, C., Kaplan, M.R., Naylor, M., Xu, S.,
2009. Middle Pleistocene glaciation in Patagonia dated by cosmogenic-nuclide
measurements on outwash gravels. Earth Planet. Sci. Lett. 286, 184–197.

Hein, A.S., Hulton, N.R.J., Dunai, T.J., Sugden, D.E., Kaplan, M.R., Xu, S., 2010. The
chronology of the Last Glacial Maximum and deglacial events in central
Argentine Patagonia. Quaternary Sci. Rev. 29, 1212–1227.

Heine, K., 1994. The late-glacial moraine sequences in Mexico: Is there evidence for a
Younger Dryas event? Palaeogeogr. Palaeoclim. Palaeoecol. 112, 113–123.

Helmens, K.F., 1990. Neogene-Quaternary geology of the High Plain of Bogota, Eastern
Cordillera, Colombia. Dissertationes Botanicae 163, 202.

Helmens, K.F., Kuhry, P., 1995. Glacier fluctuations and vegetation change associated
with late Quaternary climatic oscillations in the Andes near Bogota, Colombia.
Quaternary South Am. 9, 117–140.

Helmens, K.F., Rutter, N.W., Kuhry, P., 1997. Glacier fluctuations in the eastern Andes
of Colombia (South America) during the last 45,000 radiocarbon years. Quatern.
Int. 38–39, 39–48.

Horn, S.P., 1989. Postfire vegetation development in the Costa Rican Páramos. Madroño
36, 93–113.

Horn, S.P., 1990. Timing of deglaciation in the Cordillera de Talamanca, Costa Rica.
Clim. Res. 1, 81–83.

Horn, S.P., 1993. Postglacial vegetation and fire history in the Chirripó Páramo of Costa Rica. Quaternary Res. 40, 107–116.

Horn, S.P., 1998. Fire management and natural landscape in the Chirripó Páramo, Chirripó National Park, Costa Rica. In Nature's Geography, Zimmerer, K.S., Young, K.R. (Eds), University of Wisconsin Press.

Horn, S.P., Orvis, K.H., Haberyan, K.A., 2005. Limnology of glacial lakes in the Chirripó Paramo of Costa Rica. In Los Páramos de Costa Rica, Kappelle, M., Horn, S.P. (Eds.), Santo Domingo, Costa Rica: INBIO Press.

Ivy-Ochs, S., Kerschner, H., Schlüchter, C., 2007. Cosmogenic nuclides and the dating of lateglacial and early Holocene glacier variations: the Alpine perspective. Quatern. Int. 164–165, 53–63.

Jomelli, V., Favier, V., Vuille, M., Braucher, R., Martin, L., Blard, P.-H., Colose, C., Brunstein, D., He, F., Khodri, M., Bourlès, D.L., Leanni, L., Rinterknecht, V., Grancher, D., Francou, B., Ceballos, J.L., Fonseca, H., Liu, Z., Otto-Bliesner, B.L., 2014. A major advance of tropical Andean glaciers during the Antarctic cold reversal. Nature 513, 224–228.

Kaplan, M.R., Coronato, A., Hulton, N.R.J., Rabassa, J.O., Kubik, P.W., Freeman, S.P.H.T., 2007. Cosmogenic nuclide measurements in southernmost South America and implications for landscape change. Geomorphology 87, 284–301.

Kaplan, M.R., Fogwill, C.J., Sugden, D.E., Hulton, N.R.J., Kubik, P.W., Freeman, S.P.H.T., 2008. Southern Patagonia glacial chronology for the Last Glacial period and implications for Southern Ocean climate. Quaternary Sci. Rev. 27, 284–294.

Kaplan, M.R., Strelin, J.A., Schaefer, J.M., Denton, G.H., Finkel, R.C., Schwartz, R., Putnam, A.E., Vandergoes, M.J., Goehring, B.M., Travis, S.G., 2011. In-situ cosmogenic ^{10}Be production rate at Lago Argentino, Patagonia: Implications for late-glacial climate chronology. Earth Planet. Sc. Lett. 309, 21–32.

Kaser, G., Osmaston, H., 2002. Tropical Glaciers. Cambridge, UK: Cambridge University Press.

Kull, C., Imhof, S., Grosjean, M., Zech, R., Veit, H., 2008. Late Pleistocene glaciation in the Central Andes: Temperature versus humidity control – A case study from the eastern Bolivian Andes (17°S) and regional synthesis. Global Planet. Change 60, 148–164.

Kurz, M.D., Colodner, D., Trull, T.W., Moore, R.B., O'Briend, K., 1990. Cosmic ray exposure dating with in situ produced cosmogenic ^{3}He: Results from young Hawaiian lava flows. Earth Planet. Sc. Lett. 97, 177–189.

Laabs, B.J.C., Munroe, J.S., Best, L.C., Caffee, M.W., 2013. Timing of the last glaciation and subsequent deglaciation in the Ruby Mountains, Great Basin, USA. Earth Planet. Sc. Lett. 361, 16–25.

Lachinet, M.S., Seltzer, G.O., 2002. Late Quaternary glaciation of Costa Rica. Geol. Soc. Am. Bull. 114, 547–558.

Lachinet, M.S., Vazquez-Selem, L., 2005. Last glacial maximum equilibrium line altitudes in the CircumCaribbean (Mexico, Guatemala, Costa Rica, Colombia, and Venezuela). Quatern. Int. 138–139, 129–144.

Lachinet, M.S., Roy, A.J., 2011. Costa Rica and Guatemala. In Ehlers, J., Gibbard, P.L. (Eds.), Developments in Quaternary Science. Elsevier, Amsterdam 15, 843–848.

Lal, D., Peters, B., 1967. Cosmic ray produced radioactivity on Earth. In Encyclopedia of
Physics, Sitte, K. (Ed.), Cosmic Rays II. Springer-Verlag, New York 46, 551–612.

Lane, C.S., Horn, S.P., Mora, C.L., Orvis, K.H., Finkelstein, D.B., 2011. Sedimentary
stable carbon isotope evidence of late Quaternary vegetation and climate change
in highland Costa Rica. J. Paleolimnol. 45, 323–338.

Lane, C.S., Horn, S.P., 2013. Terrestrially derived *n*-alkane δD evidence of shifting
Holocene paleohydrology in highland Costa Rica. Arct. Antarct. Alp. Res. 45,
342–349.

Lea, D.W., Pak, D.K., Spero, H.J., 2000. Climate impact of late Quaternary equatorial
Pacific sea surface temperature variations. Science 289, 1719–1724.

League, B.L., Horn, S.P., 2000. A 10000 year record of Páramo fires in Costa Rica. J.
Trop. Ecol. 16, 747–752.

Lee, K.E., Slowey, N.C., 1999. Cool surface waters of the subtropical North Pacific
Ocean during the last glacial. Nature 397, 512–514.

Li, Y., 2013. Determining topographic shielding from Digital Elevation Models for
cosmogenic nuclide analysis: a GIS approach and field validation. J. Mt. Sci., 10,
355–362.

Li, Y., Liu, G., Chen, Y., Li, Y., Harbor, J., Stroeven, A.P., Caffee, M., Zhang, M., Li, C.,
Cui, Z., 2014. Timing and extent of Quaternary glaciations in the Tianger Range,
eastern Tian Shan, China, investigated using [10]Be surface exposure dating.
Quaternary Sci. Rev. 98, 7–23.

Licciardi, J. M., Denoncourt, C.L., Finkel, R.C., 2008. Cosmogenic [36]Cl production rates
from Ca spallation in Iceland. Earth Planet. Sc. Lett. 267, 365–377.

Licciardi, J.M., Pierce, K.L., 2008. Cosmogenic exposure-age chronologies of Pinedale and Bull Lake glaciations in greater Yellowstone and the Teton Range, USA. Quaternary Sci. Rev. 27, 814–831.

Licciardi, J.M., Schaefer, J.M., Taffart, J.R., Lund, D.C., 2009. Holocene glacier fluctuations in the Peruvian Andes indicate northern climate linkages. Science 325, 1677–1679.

Lifton, N., Smart, D.F., Shea, M.A., 2008. Scaling time-integrated in situ cosmogenic nuclide production rates using a continuous geomagnetic model. Earth Planet. Sc. Lett. 268, 190–201.

Lifton, N., Sato, T., Dunai, T.J., 2014. Scaling in situ cosmogenic nuclide production rates using analytical approximations to atmospheric cosmic-ray fluxes. Earth Planet. Sc. Lett. 386, 149–160.

Liu, B., Phillips, F.M., Fabryka-Martin, J.T., Fowler, M.M., Stone, W.D., 1994. Cosmogenic ^{36}Cl accumulation in unstable landforms 1. Effects of the thermal neutron distribution. Water Resour. Res. 30, 3115–3125.

Lozano-Garcial, S., Vazquez-Selem, L., 2005. A high-elevation Holocene pollen record from Iztaccíhuatl Volcano, central Mexico. Holocene 15, 329–338.

Martinson, D.G.N., Pisias, G., Hays, J.D., Imbrie, J., Moore, T.C. Jr., Shackleton, N.J., 1987. Age dating and the orbital theory of the Ice Ages: Development of a high-resolution 0 to 300,000-year chronostratigraphy. Quaternary Res. 27, 1–29.

Mark, B.G., Harrison, S.P., Spessa, A., New, M., Evans, D.J.A., Helmens, K.F., 2005. Tropical snowline changes at the last glacial maximum: a global assessment. Quatern. Int. 138–139, 168–201.

North Greenland Ice Core Project members, 2004. High-resolution record of Northern
Hemisphere climate extending into the last interglacial period. Nature 431, 147–
151.

North Greenland Ice Core Project members, 2004. North Greenland Ice Core Project
Oxygen Isotope Data. World Data Center for Paleoclimatology. Data
Contribution Series #2004–059. NOAA/NGDC Paleoclimatology Program,
Boulder CO, USA.

Orvis, K.H., 2002. GPS Locations and Costa Rican Topo Maps. Unpublished report.
Department of Geography, University of Tennessee, Knoxville, Tennessee. 23 pp.
http://trace.tennessee.edu/utk_geogpubs/5/

Orvis, K.H., Horn, S.P., 2000. Quaternary Glaciers and Climate on Cerro Chirripo, Costa
Rica. Quaternary Res. 54, 24–37.

Owen, L.A., Finkel, R.C., Minnich, R.A., Perez, A.E., 2003. Extreme southwestern
margin of late Quaternary glaciation in North America: Timing and controls.
Geology 31, 729–732.

Phillips, F.M., Leavy, B.D., Jannik, N.O., Elmore, D., Kubik, P.W., 1986. The
accumulation of cosmogenic chlorine-36 in rocks: a method for surface exposure
dating. Science 231, 41–43.

Phillips, F.M., Stone, W.D., Fabryka-Martin, J.T., 2001. An improved approach to
calculating low-energy cosmic ray neutron fluxes near the land/atmosphere
interface. Chem. Geol. 175, 689–701.

Phillips, F.M., Caffee, M., Dunai, T., Jull, T., Kurz, M., Schaefer, J., Stone, J., 2002. CRONUS: cosmic-ray produced nuclide systematics on earth project. Version 1.0; http://web1.ittc.ku.edu:8888/html/latest/cl/.

Phillips, F.M., Zreda, M., Plummer, M.A., Elmore, D., Clark, D.H., 2009. Glacial geology and chronology of Bishop Creek and vicinity, eastern Sierra Nevada, California. Geol. Soc. Am. Bull. 121, 1013–1033.

Pigati, J.S., Lifton, N.A., 2004. Geomagnetic effects on time-integrated cosmogenic nuclide production with emphasis on in situ ^{14}C and ^{10}Be. Earth Planet. Sc. Lett. 226, 193–205.

Pigati, J.S., Zreda, M., Zweck, C., Almasi, P.F., Elmore, D., Sharp, W.D., 2008. Ages and inferred causes of late Pleistocene glaciations on Mauna Kea, Hawai'i. J. Quaternary Sci. 23, 683–702.

Porter, S.C., 2001. Snowline depression in the tropics during the Last Glaciation. Quaternary Sci. Rev. 20, 1067–1091.

Reimer, P.J., Bard, E., Bayliss, A., Beck, J.W., Blackwell, P.G., Ramsey, C.B., Buck, C.E., Cheng, H., Edwards, R.L., Friedrich, M., Grootes, P.M., Guilderson, T.P., Haflidason, H., Hajdas, I., Hatté, C., Heaton, T.J., Hoffmann, D.L., Hogg, A.G., Hughen, K.A., Kaiser, K.F., Kromer, B., Manning, S.W., Niu, M., Reimer, R.W., Richards, D.A., Scott, E.M., Southon, J.R., Staff, R.A., Turney, C.S.M., van der Plicht, J., 2013. INTCAL13 and MARINE13 Radiocarbon age calibration curves 0–50,000 years cal BP. Radiocarbon 55, 1869–1887.

Rood, D.H., Burbank, D.W., Finkel, R.C., 2011. Chronology of glaciations in the Sierra Nevada, California, from [10]Be surface exposure dating. Quaternary Sci. Rev. 30, 646–661.

Roy, A.J., Lachinet, M.S., 2010. Late Quaternary glaciation and equilibrium-line altitudes of the Mayan Ice Cap, Guatemala, Central America. Quaternary Res. 75, 1–7.

Sato, T., Yasuda, H., Niita, K., Endo, A., Sihver, L., 2008. Development of PARMA: PHITS-based analytical radiation model in the atmosphere. Radiat. Res. 170, 244–259.

Schaefer, J.M., Denton, G.H., Barrell, D.J.A., Ivy-Ochs, S., Kubik, P.W., Andersen, B.G., Phillips, F.M., Lowell, T.M., Schluchter, C., 2006. Near-synchronous interhemispheric termination of the Last Glacial Maximum in mid-latitudes. Science 312, 1510–1513.

Schimmelpfennig, I., Benedetti, L., Finkel, R., Pik, R., Blard, P.H., Bourlès, D., Burnard, P., Williams, A., 2009. Sources of in-situ [36]Cl in basaltic rocks. Implications for calibration of production rates. Quat. Geochronol. 4, 441–461.

Schubert, C., 1988. Climatic changes during the last glacial maximum in north South American and the Caribbean: A review. Interciencia 13, 128–137.

Seltzer, G.O., 1994. Climatic interpretation of alpine snowline variations on millennial time scales. Quaternary Res. 41, 154–159.

Seltzer, G.O., 2001. Late Quaternary glaciation in the Tropics: Future research directions. Quaternary Sci. Rev. 20, 1063–1066.

Seltzer, G. O., Rodbell, D.T., Baker, P.A., Fritz, S.C., Tapia, P.M., Rowe, H.D., Dunbar, R.B., 2002. Early warming of tropical South America at the last glacial–interglacial transition. Science 296, 1685–1686.

Smith, C.A., Lowell, T.V., Caffee, M.W., 2009. Lateglacial and Holocene cosmogenic surface exposure age glacial chronology and geomorphological evidence for the presence of cold-based glaciers at Nevado Sajama, Bolivia. J. Quaternary Sci. 24, 360–372.

Smith, J.A., Farber, D.L., Finkel, R.C., Seltzer, G.O., Rodbell, D.T., 2002. Geol. Soc. Am. Annu. Meeting Progr. 34, 131.

Smith, J.A., Seltzer, G.O., Farber, D.L., Rodbell, D.T., Finkel, R.C., 2005. Early local last glacial maximum in the Tropical Andes. Science 308, 678–681.

Smith, J.A., Mark, B.G., Rodbell, D.T., 2008. The timing and magnitude of mountain glaciation in the tropical Andes. J. Quaternary Sci. 23, 609–634.

Smith, J.A., Rodbell, D.T., 2010. Cross-cutting moraines reveal evidence for North Atlantic influence on glaciers in the Tropical Andes. J. Quaternary Sci. 25, 243–248.

Stuiver, M., Reimer, P.J., 1993. Extended ^{14}C database and revised CALIB radiocarbon calibration program. Radiocarbon 35, 215–230.

Swanson, T.W., Caffee, M.L., 2001. Determination of ^{36}Cl production rates derived from the well-dated deglaciation surfaces of Whidbey and Fidalgo Islands, Washington. Quaternary Res. 56, 366–382.

Thompson, L.G., Mosley-Thompson, E., Davis, M.E., Lin, P-N., Henderson, K.A., Cole-Dai, J., Bolzan, J.F., Liu, K-B., 1995. Late Glacial Stage and Holocene tropical ice core records from Huscarán, Peru. Science 269, 46–50.

Thompson, L.G., Yao, T., Davis, M.E., Henderson, K.A., Mosley-Thompson, E., Lin, P.N., Beer, J., Synal, H. -A., Cole-Dai, J., Bolzan, J.F., 1997. Tropical climate instability: The last glacial cycle from a Qinghai-Tibetan ice core. Science 276, 1821–1825.

Thompson, L.G., Davis, M.E., Thompson, E.M., Sowers, T.A., Henderson, K.A., Zagorodnov, V.S., Lin, P.N., Mikhalenko, V.N., Campen, R.K., Bolzan, J.F., Cole-Dai, J., Francou, B., 1998. A 25,000 year tropical climate history from Bolivian ice cores. Science 282, 1858–1864.

Thompson, L.G., 2001a. Sajama Ice Core Data. World Data Center A for Paleoclimatology. Data Contribution Series #2001–009. NOAA/NGDC Paleoclimatology Program, Boulder CO, USA.

Thompson, L.G., 2001b. Huscarán Ice Core Data. World Data Center A for Paleoclimatology. Data Contribution Series #2001–008. NOAA/NGDC Paleoclimatology Program, Boulder CO, USA.

Thompson, L.G., Mosley-Thompson, E., Davis, M.E., Lin, P. -N., Henderson, K., Mashiotta, T.A., 2003. Tropical glacier and ice core evidence of climate change on annual to millennial time scales. Climatic Change 59, 137–155.

Thompson, L.G., 2004. Guliya, China Ice Core Oxygen Isotope Data. World Data Center for Paleoclimatology. Data Contribution Series #2004–057. NOAA/NGDC Paleoclimatology Program, Boulder CO, USA.

Thouret, J.C., Van Der Hammen, T., Salomons, B., 1996. Paleoenvironmental changes

and glacial states of the last 50,000 years in the Cordillera Central, Colombia.

Quaternary Res. 46, 1–18.

Vazquez-Selem, L., 2000. Late Quaternary glacial chronology of Iztaccíhuatl volcano,

central Mexico. A record of environmental change in the border of the tropics.

Unpublished Ph.D. Dissertation, Arizona State University.

Vazquez-Selem, L. and Heine, K., 2004. Late Quaternary glaciation in Mexico. In Ehlers,

J., Gibbard, P.L. (Eds.), Quaternary Glaciations-Extent and Chronology. Part III.

Elsevier, Amsterdam, pp. 233–242.

Wesnousky, S.G., Aranguren, R., Rengifo, M., Owen, L.A., Caffee, M.W., Murari, M.K.,

Perez, O.J., 2012. Toward quantifying geomorphic rates of crustal displacement,

landscape development, and the age of glaciation in the Venezuelan Andes.

Geomorphology 141–142, 99–113.

Weyl, R., 1956a. Spuren eiszeitlicher vergletscherung in der Cordillera de Talamanca

Costa Rica (Mittelamerika). Neues Jahrbuch für Geologie und Palaontologie. 102,

283–294.

Weyl, R., 1956b. Eiszeitliche gletscherspuren in Costa Rica (Mittelamerika). Zeitschrift

für Gletscherkunde und Glazialgeologie. 3, 317–325.

Young, N.E., Briner, J.P., Kaufman, D.S., 2009. Late Pleistocene and Holocene

glaciation of the Fish Lake valley, northeastern Alaska Range, Alaska. J.

Quaternary Sci. 24, 677–689.

Young, N.E., Briner, J.P., Leonard, E.M., Licciardi, J.M., Lee, K., 2011. Addressing climatic and nonclimatic forcing of Pinedale glaciation and deglaciation in the western United States. Geology 39, 171–174.

Zech, R., Kull, C., Veit, H., 2006. Late Quaternary glacial history in the Encierro Valley, northern Chile (29°S), deduced from [10]Be surface exposure dating. Palaeogeogr. Palaeoclim. Palaeoecol. 234, 277–286.

Zech, R., May, J-H., Kull, C., Ilgner, J., Kubik, P.W., Veit, H., 2008. Timing of the late Quaternary glaciation in the Andes from ~15 to 40° S. J. Quaternary Sci. 23, 635–647.

Zech, J., Zech, R., Kubik, P.W., Veit, H., 2009. Glacier and climate reconstruction at Tres Lagunas, NW Argentina, based on [10]Be surface exposure dating and lake sediment analyses. Palaeogeogr. Palaeoclim. Palaeoecol. 284, 180–190.

Zreda, M.G., Phillips, F.M., Elmore, D., Kubik, P.W., Sharma, P., Dorn, R.I., 1991. Cosmogenic chlorine-36 production rates in terrestrial rocks. Earth Planet. Sc. Lett. 105, 94–109.

APPENDICES

APPENDIX A

Cosmogenic ^{36}Cl Nuclide Sample Processing Laboratory Procedure

Whole Crushed Rock Sample Processing for Chlorine-36 Analysis

University of Tennessee

Department of Geography

Science and Engineering Research Facility (SERF), Room 421

Procedure based off Cosmogenic ^{36}Cl Nuclide Sample Processing Procedure from

PRIME Lab at Purdue University and modified for the Cosmogenic Sample Processing

Laboratory at the University of Tennessee

Table A1: Cosmogenic ^{36}Cl nuclide sample processing bench sheet.

SAMPLE ID:

Location:

Longitude/Latitude:

Date Chemistry Started:

Processed by:

DISSOLUTION

Carrier Concentration (mg/g):

Wt. of Leached Rock:

Amt. of Carrier (mg)*:

Wt. added carrier (g):

Date Dissolution Started:

Date Fully Dissolved:

CENTRIFUGATION

Centrifuge Bottle Wt.:

Date Refrigerated:

Date Removed:

Column # Used:

FINAL SAMPLE PREPARATION

Final Wt. (with Tube) (g):

Tube Tare Weight (g):

AgCl Weight (mg):

Cl Weight (mg)**:

* = Weight of Added Carrier (g) X Carrier Concentration

** = AgCl weight X 0.24735

Sample Notes:

Table A2: Volumetric/mass amounts for mixing solutions.

Solutions		
Concentration	**Material**	**Units**
3% HNO3 Leaching Solution*		
10 L Solution:	Fisher Reageant Grade Nitric Acid	300 g HNO3: Pure Water
* 3% HNO3 is recycled and should be dumped into corresponding waste container		
10% HNO3		
10 L Solution:	Fisher Reageant Grade Nitric Acid	1000 g HNO3: Pure Water
* 3% HNO3 is recycled and should be dumped into corresponding waste container		
0.1 M	Alfa Aesar Metals Basis 99.9994% pure Silver Nitrate (granular)	0.16787 g/mL
0.05 M	Fisher TraceMetal Grade Nitric Acid stock solution (70% w/w)	3.185 mL/L
0.15 M	Fisher TraceMetal Grade Nitric Acid stock solution (70% w/w)	9.556 mL/L
1.5 M	Fisher TraceMetal Grade Nitric Acid stock solution (70% w/w)	95.557 mL/L
4.0 M	Fisher TraceMetal Grade Nitric Acid stock solution (70% w/w)	254.818 mL/L
30%	Fisher TraceMetal Grade Ammonium Hydroxide stock solution (30% w/w)	
0.15 M	Fisher TraceMetal Grade Ammonium Hydroxide stock solution (30% w/w)	19.472 mL/L
Carrier		
1.0000 mg/g	Ammonium Chloride (NH4Cl) Stable Carrier (granular)	0.001 g

LABORATORY EQUIPMENT

Barnstead Millipore Water Filtration System

When refilling the pure 18 Ω H_2O carboy:

- Turn the faucet connected to the filtration system a quarter of an inch away from you to start feeding water into the filtration system.

- Push the "Start/Stop" button on the panel to exit "Standby" mode.

- Once the panel reads 18.2 Ω, turn the switch on top of the filtration to the right to sustain dispense mode.

- Make sure that the designated pure 18 Ω H_2O 1 L graduated cylinder is underneath the dispensing spigot.

- If needed, continue to dispense water into the graduated cylinder and dump into the pure 18 Ω H_2O carboy until the carboy is filled.

- When you are done using the water filtration system, push the "Standby" button and turn the faucet off.

While dispensing, make sure that the water stays at 18.2 Ω. If it goes below this, stop dispensing and wait until the panels reads 18.2 Ω again. If the water frequently goes below 18.2 Ω, this may indicate that the water going into the system is at too high pressure. To fix this, turn the water pressure down by turning the faucet slightly towards you. However, take caution with turning the water levels down too much. You should not see air bubbles in the water tube connecting the faucet to the filtration system.

IEC Centrifuge

- This centrifuge is used frequently for cosmogenic [36]Cl sample processing. 1 Liter centrifuge bottles and 50 mL centrifuge tubes are used in this centrifuge. The 50 mL centrifuge tube adapters are located in the cabinet above the desk.

- Specific instructions for operating the centrifuge are located on the centrifuge lid. Refer to those before using the centrifuge, and have a senior lab worker assist you during your first use.

- This centrifuge is old and has a tendency to stop during use. If this occurs, turn the speed and timer off. Wait for the rotor to completely stop before turning the brake on and opening the centrifuge.

- Always take the adapters out of the holders after each use. If you do not, the centrifuge will become corroded and lead to expensive repairs. After taking the adapters out, carefully rinse them three times with pure 18 Ω H_2O and Kimwipes, dry them, and place them back into the cabinet.

- When using the centrifuge, make sure the bottles are of equal weight and are evenly distributed. Always make sure there is a bottle of equal weight directly across from another bottle. Uneven distribution of the bottles will cause the centrifuge to become unbalanced and need repairs.

Isotemp Oven

- This oven is for drying samples. Make sure that the door is always tightly shut. If the oven appears to be dirty, wipe the shelves and sides down with pure 18 Ω H_2O and Kimwipes. Ask a senior lab worker for assistance if the shelves need to be taken out or adjusted.

CAUTION: This oven runs ~40 °C higher than the set temperature. For example, if the temperature dial reads 20 °C, it will actually be about 60 °C.

MAKE SURE YOU KEEP THIS IN MIND FOR THE REMAINDER OF THE PROCEDURE. IF SET ON ACTUAL TEMPERATURE, SAMPLE BOTTLES WILL MELT. THIS WILL RUIN YOUR SAMPLE AND DAMAGE THE OVEN.

Igloo Refrigerator

- Refrigerator use is rather basic. You will store your samples in here during the process. If there are any problems with temperature or maintenance, please notify a senior lab worker.

Make sure to keep the refrigerator clean to avoid contamination. Samples should always be placed in the refrigerator with lids tightly sealed.

VWR Vortex

- The VRW Vortex is used to mix the sample before placing the sample into the IEC Centrifuge. This step assures that unwanted material that might have settled on the bottom of the centrifuge tube will not settle with the sample when centrifuged. When using the Vortex, make sure that the cap on the centrifuge tube is tightly sealed and no liquid is on the outside of the tube before placing into the centrifuge.

Mini centrifuge

- The mini centrifuge is used during final sample preparation. Carefully load the mini centrifuge tubes containing the samples into the holder. Make sure that the centrifuge is balanced. If you have an odd number of samples, make sure to use a blank tube on the opposing side. Fill the blank tube with water before hand to assure that it is near a similar weight to the tube containing your sample.

Sample Leaching

10% HNO_3

<div align="center">

70 mL pure18 Ω H_2O

7 mL of Reagent Grade (RG) HNO_3
</div>

Dish Washing

Nalgene and Centrifuge Bottles

3% HNO_3

Always leach the Nalgene bottles and centrifuge bottles before use. When in doubt, 3% leach the container before use. If the carboy labeled "3% HNO_3 Leaching" in the fume hood is empty, mix the following:

<div align="center">

For a 10 L Solution:
</div>

300 g Reagent Grade (RG) HNO₃: 18 Ω H₂O

If you want to make a 20 L solution in the carboy, simply double the amount of both HNO₃ and pure 18 Ω H₂O.

Make sure the carboy is empty before refilling. If it is not empty, the concentrations will be skewed.
Always use Reagent Grade (RG) HNO₃ when making this solution
The 300 g of HNO₃ can be weighed out on the Ohaus 2000 g balance in the right fume hood.
ALWAYS MAKE SURE TO THOROUGHLY TRIPLE RINSE THE BOTTLES AFTER LEACHING. The RG HNO₃ contains high chlorine amounts, which will contaminate the sample.

SAMPLE PROCESSING

1. Crushed Rock Sample Leaching

Make sure not to mix up the samples during this step. Try to keep the samples organized with corresponding bottles lids.

- Reserve ~10 grams of crushed rock sample for whole rock analysis in 15 mL Nalgene sample vial labeled with sample ID and "before." Set this sample aside.
- Using the Ohaus 2000 g balance in the right fume hood, tare a 250 mL Nalgene bottle that has been leached with 3% nitric acid (HNO₃) solution for one or more hour and triple rinsed with pure 18 Ω water. Label the bottle and the corresponding cap with the sample ID.
- Add 80 grams of crushed rock sample to the corresponding tared bottle (leave the cap off) on the balance.
- Repeat this step for each sample.
- Add 70 mL of pure 18 Ω water to each sample bottle.

CAUTION: Perform the following step carefully. Reactive components of the rock sample such as carbonate or other strongly basic salts may cause a vigorous reaction when the nitric acid is introduced. Transfer the acid solution with caution!

- Carefully add 7 mL of stock reagent grade (RG) nitric acid solution to the sample bottle
- Momentarily leave the cap loose and wait for any reaction or outgassing to cease before proceeding.

Both Reagent grade (RG) and Trace Metal Grade (TMG) nitric acid can be found in the laboratory. (RG) HNO$_3$ should be used for this portion of the procedure. (TMG) HNO$_3$ is only for separation and purification operations as detailed later in this procedure.

- Tighten the cap and vigorously swirl the mixture of sample and nitric acid solution for 5 to 10 seconds, then re-loosen the cap.
- Leave the samples in the fume hood overnight (12 to 16 hours).

2. Leached Rock Sample Washing and Drying

- Decant the acid solution into the suitable acidic waste container.
- Rinse the fines from the rock sample by adding pure 18Ω water to the sample bottle, closing the bottle, and swirling vigorously for 5 to 10 seconds.

Filling the bottle about 2/3 or 3/4 of the way full with water should be sufficient for a rinse.

- Decant the supernatant water from the bottle into the acid waste container.
- Repeat steps 13 and 14 at least four more times until the rinse water is reasonably clear and free of fine particles.
- Uncap the bottle and place it horizontally on the drying rack in a drying oven. Place the cap next to or near the bottle in the oven.
- Dry the samples at 20 °C overnight (12 to 16 hours).

- Collect approximately 10 g of the leached and dried rock sample in a Nalgene 15 mL plastic vial and label it with the PRIME Lab SID and "After"

20 °C overnight because the oven runs 40 °C warmer than it reads

3. Rock Sample Carrier Addition and Digestion

- Tare a clean, acid leached plastic 500 mL bottle with a powder funnel in the mouth on the Mettler Toledo analytical balance.
- Add 30 g of leached and dried rock sample. Record the exact weight on the Cosmogenic ^{36}Cl Nuclide Sample Processing bench sheet.
- Remove the powder funnel.
- Re-tare the balance.
- Add 1 g of approximately 1.000 (mg/g) Chlorine-35 enriched (or "spike") carrier solution with a clean, disposable transfer pipette. Record the exact weight and concentration of carrier solution added on the bench sheet, as this will be used for calculating the exact amount of pure carrier present in the sample in milligrams.

The concentration of the carrier solution is written on the carrier bottle.

- **Carefully** move the sample bottle containing the rock sample and the carrier solution to a fume hood containing a balance.
- Tare the bottle containing the 30 g sample and the 1 g of carrier solution on the balance in the fume hood.
- Add 150 g (or 5 times the weight of the sample) of pure 18 Ω water.
- Carefully add 150 g (or 5 times the weight of the sample) of low chloride 40% hydrofluoric acid solution.
- Add 45 g (or 1.5 times the sample weight) of concentrated TMG HNO_3.

In step (29), Trace Metal Grade (TMG) nitric acid is required to minimize the contaminants, which may be present in RG nitric acid solution. ALWAYS USE TRACE METAL GRADE FOR THIS STEP.

- Tightly cap the bottle and agitate to expose all surfaces of the rock sample to the solvent acid solution.
- Once the bottle has cooled to room temperature, transfer the bottle to the hot dog roller in the fume hood. Note the time and date the bottles were put onto the hot dog roller to heat setting 4 (to the permanent marker line).
- Place the bottles on with cap facing to the right.
- After an hour, check the hot dog roller to make sure none of the samples are leaking or expanding.
- Continue to periodically check samples on the hot dog roller every 4–6 hours. Do not turn temperature down overnight because bottles will implode.
- If the samples have not dissolved by nighttime, carefully take the samples off of the hot dog roller and loosen the cap on the bottle. Return in the morning to tightly cap the bottles and place back onto the hot dog roller.

Complete dissolution of the sample with HF/HNO3 may take longer than 48 hours. The length of time required varies with the type of rock, which comprises the sample.

Complete digestion of rock samples may still leave insoluble fluoride compounds as fine sediment or residue in the bottom of the digestion bottle. This is normal, and upon complete digestion is normally a white or off-white color.

- To see if the sample is completely dissolved, hold the tightly capped bottle up to the light and swirl the sample. If you see any dark material, the sample needs to dissolve longer.
- If no dark material is seen, take the bottle off of the hot dog roller and loosen the cap to let the sample cool.
- Note the day and time of dissolution of each sample.
- Carefully transfer the contents of the bottle to a clean 1 liter centrifuge bottle.
- If more than one sample is being processed, weigh each sample-filled centrifuge bottle on the balance in the nitric acid fume hood. Note the weight of the heaviest centrifuge bottle.

- Add pure 18 Ω water from a water wash squeeze-bottle or disposable transfer pipette to each other centrifuge bottle until they are all within ±0.05 g of one another.

CAUTION: Failure to equalize the weights of each centrifuge bottle will cause the centrifuge to become unbalanced. This step is extremely important to the safe and proper operation of the centrifuge.

- Centrifuge the samples in the IEC Centrifuge bottles at 67% speed (~2350 rpm) for 40 minutes.

4. Initial Precipitation and Separation of Silver Chloride

- Decant the supernatant liquid into a pre-leached 18 Ω water rinsed 500 mL Nalgene plastic bottle.
- Add 10 drops of silver nitrate ($AgNO_3$) solution and swirl the bottle.
- Allow the samples to sit tightly capped for 1 to 2 hours.
- Place the bottle in the refrigerator overnight (for 12 to 16 hours) to allow the silver chloride precipitate to settle to the bottom of the bottle.
- Remove the bottle from the refrigerator and **carefully (without disturbing the solid at the bottom)** decant the top layer of supernatant liquid into a 1 L Nalgene Silver Waste bottle.

Have a senior lab worker show you how to do the above step your first time.

- Transfer the remaining liquid and suspended solids into a pre-leached 50 mL Falcon centrifuge tube. Make sure the tube has been leached with 3% HNO_3 and triple rinsed three times before use.
- Wash any residual solids out of the bottle with a few milliliters of pure 18 Ω water and decant into the centrifuge tube.
- Place the black 50 mL centrifuge tube adapters into the IEC centrifuge.
- Cap the centrifuge tube and centrifuge at 67% speed (~2350 rpm) for 40 minutes.

- Remove the tube from the centrifuge tube and carefully decant the waste into a silver waste container

  If material does not look compact at bottom of centrifuge tube, the sample may need to be centrifuged for an additional 10–20 minutes.

- Add 5 mL of 18 MΩ water to the 50 mL centrifuge tube to rinse the precipitate.

- Cap the tube and vortex the sample with water for 10 seconds on high using the VWR Analog Vortex Mixer.

- Centrifuge the mixed sample again at 67% speed (~2350 rpm) for 40 minutes.

- Remove the centrifuge tube from the centrifuge and decant the waste into the silver waste container.

The sample is now ready for ion exchange column purification.

5. Anion Exchange Column Preparation and Conditioning

The column preparation procedure is only necessary if the columns are not already assembled. However, the condition procedure should be performed before using the columns, and again after using the columns in the case that the resin packing will be reused for further samples. If the column is already packed, skip to step 6.

1. To pack the column

- If a line is not already drawn on the column 5 cm from the frit at the bottom of the column, draw one with permanent black marker.

- Swirl the container of AG 1-X8 anion exchange resin in water vigorously, then quickly pour about 50 mL into a plastic 100 mL beaker.

- Draw up the resin suspended in water into a plastic disposable transfer pipette and transfer the resin suspension in the column.

- Slowly swirl the resin with the pipette during transfer to reduce air bubbles in the resin.

- Open the stopcock on the column

- Transfer enough resin such that the 18 MΩ water is level with the line drawn in permanent black marker.

- Allow the water to drain from the column. Then, add more resin as needed such that the compacted, moist resin bed is level or slightly higher than the black marker line.

If the resin bed level ends up being much higher than the marker line, close the column stopcock, add water with a pipette, and then agitate the water and resin bed by rapidly drawing up water and re-depositing it back in the column. This will cause the resin to go into a suspension temporarily. Draw up some of that suspension and transfer it back to the beaker containing the resin stock. Wait for the resin bed to settle once again and agitate and draw up more as needed.

Once the resin bed has settled to the level indicated by the maker line, the column is now assembled and ready for conditioning.

2. To condition the column
- Pass an 8 mL aliquot of 4.0 M nitric acid solution through each column, and drain into a 250 mL Nalgene bottle labeled "Anion Exchange Conditioning."
- Place the yellow 250 mL cup atop the column and ensure a snug fit with the collar of the column.
- Transfer 20 mL of pure 18 Ω water to the column with a graduated cylinder and drain the water through the column into the 250 mL Nalgene bottle labeled "Anion Exchange Conditioning."

Once the 20 mL of water has drained completely, the column is conditioned and ready for sample chloride separation.

6. Sample Chloride Separation through Anion Exchange Chromatography
- To dissolve the crude silver chloride precipitate in the centrifuge tube, add 20 drops of 30% ammonium hydroxide (NH_4OH) from a dropper bottle and 5 mL of pure 18 Ω water to the centrifuge tube.

- Cap and vortex the tube using the VWR Analog Vortex Mixer for 10–15 seconds to fully dissolve the sample pellet. The sample silver chloride should now be in the solution.

If a significant quantity of solid residue remains in the tube after adding NH4OH, it is recommended that the tube be vortexed and centrifuged again AFTER the addition of ammonium hydroxide. After centrifugation, decant the supernatant solution with a transfer pipette into a new, pre-leached 50 mL centrifuge tube. DO NOT IMMEDIATELY DISPOSE OF THE RESIDUAL SOLIDS. The supernate is the solution, which should then be transferred into the column in the following step.

- Place the 250 mL silver nitrate waste bottle labeled "AgNO$_3$ Waste" under the column stopcock.
- Transfer the solution to the column and open the stopcock to elute the solution. Drain the solution to the surface of the resin bed.
- Rinse the centrifuge tube with 10 mL of 0.1 M NH$_4$OH solution, vortex and centrifuge if necessary, and then transfer the rinse to the column. Again, drain the solution to the surface of the resin bed.
- Next, add 10 mL of 0.05 M HNO$_3$ solution through each column into the silver nitrate waste bottle. Drain to the surface of the resin bed.
- Add 10 drops of AgNO$_3$ solution in a clean 50 mL centrifuge tube for each sample.
- After the 0.05 M HNO$_3$ has finished draining, close the column stopcock and remove the silver nitrate waste bottle from under the column and replace it with a 50 mL centrifuge tube containing the AgNO$_3$.
- Elute the chloride ions from the column by adding a 20 mL aliquot of 0.15 HNO$_3$ solution to the column, being sure that the centrifuge tube containing the silver nitrate is under the column before opening the stopcock.
- Drain the nitric acid solution into the centrifuge tube. After a minute or so a white turbidity should be apparent in the centrifuge tube. This is the isolated silver chloride precipitate.

Try to avoid exposing the suspension in the centrifuge tubes to direct sunlight.

- Once the elution has completed (the level of solution in the column is level with or slightly below the surface of the resin bed), add 20 drops of trace metal grade concentrated HNO_3 to the centrifuge tube from a dropper bottle.
- Cap the tube tightly and vortex for 10 seconds using the VWR Analog Vortex Mixer.
- Place the sample centrifuge tube in the refrigerator overnight to allow the precipitate to form and settle.

Be sure to recondition the columns as described in Section 5-2 (on the preceding page). After reconditioning, be sure to close the stopcock, place the waste beakers beneath the columns, and add 2 to 3 cm of pure 18 Ω water on top of the anion resin bed to keep the resin packing moist for the next use.

7. Final Sample Preparation
- Remove the sample from the refrigerator.
- Vortex the sample for 20 seconds using the VWR Analog Mixer.
- Centrifuge at 67% speed (~2350 rpm) for 40 minutes.
- Remove from the centrifuge and decant the supernatant liquid carefully into a 1 liter silver waste Nalgene bottle.
- Add 5 mL of pure 18Ω water to rinse the pellet.
- Vortex the sample for 10 seconds.
- Centrifuge the sample tube at 67% speed (~2350 rpm) for 40 minutes.
- Decant the supernatant water rinse into a 1 liter silver waste Nalgene bottle.

A. Preparing the microcentrifuge tube
- Label a mincrocentrifuge tube with the SID of the sample using an ultra-fine tipped permanent marker.
- Weight the dry microcentrifuge tube on the Mettler Toledo analytical balance to 0.0001 g and record the weight on the bench sheet in the blank for "Tare Weight."

- Triple-rinse the microcentrifuge tube with pure 18Ω water, and place in a microcentrifuge tube holder.

B. Transferring the sample

- Add pure 18 Ω water to the microcentrifuge tube up to the 1 mL gradation mark on the side of the tube.
- Transfer the water from the microcentrifuge tube into the 50 mL centrifuge tube containing the sample using a plastic disposable transfer pipette.
- Use the tip of the disposable pipette to dislodge and break up the pellet of silver chloride at the bottom of the 50 mL centrifuge tube.
- Carefully draw the precipitate in water suspension up into the transfer pipette and transfer it over into the microcentrifuge tube.
- Add approximately 0.5 mL of pure 18Ω water to the 50 mL centrifuge tube and draw that up with the transfer pipette.
- Transfer the 0.5 mL wash into the microcentrifuge tube.

Use a different disposable transfer pipette for each sample if there are multiple samples. This will avoid cross-contamination between the samples.

C. Centrifuging the sample

- Place up to 6 microcentrifuge tubes into the microcentrifuge.

If an odd number of samples are placed in the centrifuge, counterblanace microcentrifuge tubes containing pure water must be used to ensure that the centrifuge does not become unbalanced during operation.

- Turn on the power button of the mini centrifuge and centrifuge the samples for 10 minutes.
- After 10 minutes, turn off the power button on the mini centrifuge and wait for it to stop.
- Take out the samples from the mini centrifuge.

- Use a new disposable plastic transfer pipette to carefully draw up the supernatant water over the silver chloride pellet. TAKE CARE NOT TO DRAW UP THE SAMPLE PELLET AS WELL.

- Dispose of the supernatant water in a 1 liter silver waste Nalgene bottle.

D. Preparing the sample for AMS

- Place the microcentrifuge tube in the microcentrifuge tube holder.

- Open the lid of the tube and place the tube and holder in a drying oven set to 20 ^{o}C for 12 to 24 hours to dry the sample.

- Remove the dried sample from the oven and close the lid of the microcentrifuge tube.

- Allow the tube to cool, then weigh and record the weight of the tube and sample on the Mettler Toledo analytical balance. Record the weight on the bench sheet.

- Perform the calculations from the data detailed on the bench sheet.

- Input the sample IDs and necessary data into an Excel worksheet.

8. Loading the holder for AMS

You will need:

- ^{36}Cl holder (Cu covered by AgBr) – can be ordered from Purdue PRIME Lab

- #47*2 HSS Drill Blank

- Extra fine silicon carbide sandpaper

- Isopropanol alcohol

- Kimwipes

- Hammer

- Paper (8" x 11")

- Microcentrifuge tube box (1.5 mL)

- Tweezers (sterile)

- Anti-static gloves

Loading Preparation:

- The holder should be preheated at 30 ℃ in the oven for 20 minutes on a stable piece of aluminum foil.

- Start heating the vials that you will put the holder in at the beginning of loading for each sample.

- After 20 minutes, take the holder out of the oven using tweezers and place the holder on a clean surface on a piece of paper.

- **Record the holder number and sample ID (number on the bottom of the holder). This is very important and is the only way to keep track of the samples when we ship them to AMS.**

Loading Sample into Holder:

- Pour sample onto a smaller piece of paper (1" x 1")

- Transfer sample from small piece of paper onto the top of the holder

- Stabilize the holder using tweezers in one hand, and in the other hand use a clean drill blank to push the sample into the holder evenly over the holder surface.

- After the sample sticks over an even surface of the holder, take a hammer and gently pound the sample into the holder surface using a drill blank. Continue to stabilize the holder with the tweezers.

- Do not pound the sample too much, as this will make it difficult for the AMS to detect.

- Once the sample is complete, bake the holder in the oven at 30 ℃ for 10 minutes.

- After 10 minutes, use tweezers to gently place the holder into the vial (holder surface should be facing down in the vial – on the bottom of the vial).

- Screw the vial lid onto the vial and place vial into vial holder.

DOUBLE-CHECK THAT YOU HAVE RECORDED THE SAMPLE ID AND THE CORRESPONDING VIAL #. THIS IS THE ONLY WAY TO IDENTIFY YOUR SAMPLES WHEN WE GET THE AMS RESULTS.

Cleaning:

- Clean the drill blank with isopropanol alcohol using a Kimwipe, then sand the drill blank using sandpaper, and clean once more using isopropanol alcohol and a Kimwipe.

- Clean the loading surface using isopropanol alcohol and a Kimwipe.

- Clean the tweezers and hammer the same way as mentioned in the previous step.

Finished!

- Send the sample to PRIME Lab for analysis with the AMS.

APPENDIX B
Cosmogenic ^{36}Cl Nuclide Supplementary Information

Table B1: Measured ^{36}Cl concentrations and physical field data.

Sample ID	Latitude (°)	Longitude (°)	Elev. (m)	Thickness (cm)	Bulk Density (g/cm^3)	Topographic Shielding	Conc. ^{36}Cl (atoms/g)
I–2	9.452	– 83.505	3357	4.0	2.65	0.9880	237513
I–3	9.452	– 83.505	3357	4.0	2.65	0.9880	550199
I–4	9.452	– 83.505	3357	4.0	2.65	0.9880	316617
I–6	9.452	– 83.505	3357	4.0	2.65	0.9880	249605
I–7	9.452	– 83.505	3357	4.0	2.65	0.9880	288687
I–8	9.452	– 83.505	3357	4.0	2.65	0.9880	300257
I–9	9.452	– 83.505	3357	4.0	2.65	0.9880	354606
I–10	9.452	– 83.505	3357	4.0	2.65	0.9880	405835
II–2	9.453	– 83.505	3349	4.0	2.65	0.9811	224906
II–5	9.453	– 83.505	3349	4.0	2.65	0.9811	520733
II–6	9.453	– 83.505	3349	4.0	2.65	0.9811	403995
II–8	9.453	– 83.505	3349	4.0	2.65	0.9811	348130
II–9	9.453	– 83.505	3349	4.0	2.65	0.9811	371667
II–10	9.453	– 83.505	3340	4.0	2.65	0.9811	346033
2–1	9.500	– 83.489	3462	4.0	2.65	0.9870	1010266
2–2	9.500	– 83.489	3462	4.0	2.65	0.9870	593425
2–3	9.500	– 83.489	3462	4.0	2.65	0.9870	657242
2–4	9.500	– 83.489	3462	4.0	2.65	0.9870	464668
2–5	9.500	– 83.489	3462	4.0	2.65	0.9870	380778
2–6	9.500	– 83.489	3462	4.0	2.65	0.9870	1048430
2–7	9.500	– 83.489	3462	4.0	2.65	0.9870	834428
2–8	9.500	– 83.489	3462	4.0	2.65	0.9870	1023950
2–9	9.500	– 83.489	3462	4.0	2.65	0.9870	401335
2–10	9.500	– 83.489	3462	4.0	2.65	0.9870	1020543
3–1	9.505	– 83.492	3391	4.0	2.65	0.9751	1031158
3-2	9.505	– 83.492	3391	4.0	2.65	0.9751	709430
3–3	9.505	– 83.492	3391	4.0	2.65	0.9751	758216
3–5	9.505	– 83.492	3391	4.0	2.65	0.9751	1044610
3–6	9.505	– 83.492	3391	4.0	2.65	0.9751	1106328
3–7	9.505	– 83.492	3391	4.0	2.65	0.9751	999280
3–8	9.505	– 83.492	3391	4.0	2.65	0.9751	964233
3–9	9.505	– 83.492	3391	4.0	2.65	0.9751	891959
3–10	9.505	– 83.492	3391	4.0	2.65	0.9751	1145305
4–1	9.513	– 83.496	3310	4.0	2.65	0.9753	4574836
4–2	9.513	– 83.496	3310	4.0	2.65	0.9753	412998
4–3	9.513	– 83.496	3310	4.0	2.65	0.9753	1216246
4–4	9.513	– 83.496	3310	4.0	2.65	0.9753	2415086
4–5	9.513	– 83.496	3310	4.0	2.65	0.9753	1856938
4–6	9.513	– 83.496	3310	4.0	2.65	0.9753	1132525
4–7	9.513	– 83.496	3310	4.0	2.65	0.9753	998119
4–8	9.513	– 83.496	3310	4.0	2.65	0.9753	943652
4–9	9.513	– 83.496	3310	4.0	2.65	0.9753	767176
4–10	9.513	– 83.496	3310	4.0	2.65	0.9753	1192312

Table B1. Continued

Sample ID	Latitude (°)	Longitude (°)	Elev. (m)	Thickness (cm)	Bulk Density (g/cm^3)	Topographic Shielding	Conc. ^{36}Cl (atoms/g)
MOR 98–0	9.488	– 83.488	3551	4.0	2.65	0.9745	488849
MOR 98–2	9.497	– 83.488	3482	4.0	2.65	0.9886	1015314
MOR 98–3	9.496	– 83.490	3513	4.0	2.65	0.9865	537189
MOR 98–4	9.495	– 83.490	3558	4.0	2.65	0.9774	628409
MOR 98–5	9.495	– 83.491	3590	4.0	2.65	0.9947	1115174

Table B2: [36]Cl bulk rock elemental analysis (ppm).

Sample ID	Cl	B	Sm	Gd	U	Th	Cr	Li
I–2	1.4	10.0	1.1	1.3	0.1	0.1	30.0	10.0
I–3	5.1	10.0	0.5	0.7	0.1	0.2	60.0	10.0
I–4	1.1	10.0	1.4	1.6	0.2	0.3	60.0	10.0
I–6	0.3	10.0	1.7	2.2	0.3	0.3	40.0	10.0
I–7	16.1	10.0	1.3	1.7	0.3	0.2	30.0	10.0
I–8	18.1	10.0	1.7	2.0	0.2	0.3	20.0	10.0
I–9	28.2	10.0	2.5	3.1	0.4	0.8	30.0	10.0
I–10	1.3	10.0	2.1	2.5	0.3	0.3	60.0	10.0
II–2	8.2	10.0	1.7	2.1	0.2	0.2	80.0	10.0
II–5	2.9	10.0	1.8	2.2	0.2	0.3	36.0	10.0
II–6	2.8	10.0	2.2	2.5	0.3	0.5	20.0	10.0
II–8	8.9	10.0	1.4	1.8	0.2	0.2	30.0	10.0
II–9	4.1	10.0	2.1	2.6	0.3	0.5	20.0	10.0
II–10	2.0	10.0	1.4	1.7	0.2	0.2	30.0	10.0
2–1	174.6	10.0	1.4	1.2	1.0	2.4	110.0	10.0
2–2	260.2	10.0	2.9	2.8	1.0	2.3	80.0	10.0
2–3	218.0	10.0	2.5	2.8	0.9	1.8	130.0	10.0
2–4	134.4	10.0	2.9	3.4	1.5	2.1	120.0	10.0
2–5	75.4	40.0	3.9	4.1	2.2	3.0	80.0	10.0
2–6	295.6	10.0	3.0	2.9	1.1	2.3	70.0	10.0
2–7	239.9	20.0	2.0	2.0	1.1	2.0	90.0	20.0
2–8	347.4	20.0	2.5	2.4	1.1	2.0	90.0	20.0
2–9	76.2	10.0	4.0	4.0	2.0	2.7	80.0	10.0
2–10	405.7	10.0	2.5	2.6	1.2	2.6	80.0	10.0
3–1	393.2	10.0	2.2	2.5	1.3	2.5	60.0	10.0
3–2		10.0	2.3	2.4	1.2	2.3	70.0	12.5
3–3	256.2	10.0	2.2	2.3	1.2	2.4	70.0	10.0
3–5	349.8	10.0	2.3	2.2	1.2	2.3	80.0	10.0
3–6	456.7	10.0	2.5	2.5	1.2	2.5	60.0	10.0
3–7	399.1	10.0	2.3	2.5	1.2	2.2	70.0	10.0
3–8	327.2	10.0	2.3	2.3	1.2	2.3	70.0	20.0
3–9	276.7	10.0	2.2	2.4	0.9	1.9	80.0	10.0
3–10	425.5	10.0	2.2	2.4	1.3	2.5	70.0	10.0
4–1	321.7	10.0	2.4	2.5	1.0	2.0	100.0	10.0
4–2	339.0	10.0	2.2	2.3	1.0	1.5	120.0	10.0
4–3	367.3	10.0	3.5	3.6	1.0	1.4	100.0	10.0
4–4	397.6	10.0	2.6	2.7	1.1	2.0	70.0	10.0
4–5	284.9	10.0	3.2	3.3	1.7	3.0	70.0	10.0
4–6	268.5	40.0	3.2	3.3	1.4	2.8	70.0	10.0
4–7	348.9	10.0	3.1	3.1	1.0	1.7	80.0	10.0
4–8	194.8	10.0	3.2	3.3	1.2	2.4	80.0	10.0
4–9	123.1	10.0	3.1	3.0	1.3	2.6	80.0	10.0
4–10	196.4	10.0	3.2	3.3	1.1	2.3	60.0	10.0
MOR 98–0	64.0	11.0	2.0	4.0	1.0	2.0	149.0	10.0
MOR 98–2	382.3	9.0	2.0	5.0	1.0	2.0	150.0	10.0
MOR 98–3	78.4	17.0	2.0	3.0	1.0	2.0	201.0	10.0
MOR 98–4	89.1	7.0	2.0	3.0	1.0	2.0	321.0	10.0
MOR 98–5	123.1	10.0	2.0	4.0	1.0	2.0	170.0	10.0

Table B3: ^{36}Cl bulk rock elemental analysis (oxide weight %).

Sample ID	SiO$_2$	TiO$_2$	Al$_2$O$_3$	Fe$_2$O$_3$	MnO	MgO	CaO	Na$_2$O	K$_2$O	P$_2$O$_5$
I–2	65.4	0.65	10.1	7.3	0.10	2.0	5.2	3.0	0.69	0.01
I–3	79.2	0.43	6.3	4.4	0.02	0.3	2.2	1.2	0.74	0.01
I–4	52.5	0.78	15.0	11.1	0.12	6.5	8.4	1.5	0.26	0.04
I–6	47.4	0.93	19.3	11.4	0.14	5.5	8.8	3.1	0.38	0.06
I–7	50.3	0.92	19.2	11.2	0.13	4.8	7.9	2.8	0.31	0.05
I–8	49.8	0.83	18.2	10.7	0.19	4.1	8.1	2.7	0.67	0.09
I–9	50.3	0.74	18.9	9.1	0.16	2.9	8.3	3.5	1.24	0.16
I–10	45.6	0.91	18.7	12.2	0.16	5.9	11.8	2.0	0.18	0.10
II–2	47.8	0.81	17.0	11.8	0.16	6.6	10.8	2.0	0.22	0.04
II–5	49.8	0.82	18.9	10.3	0.18	4.3	9.2	2.5	0.75	0.07
II–6	50.6	0.81	19.9	9.3	0.13	3.3	8.8	2.4	0.89	0.10
II–8	52.1	0.80	17.6	10.2	0.20	4.1	7.2	3.2	0.89	0.06
II–9	48.7	0.86	20.7	10.1	0.16	3.5	9.9	2.5	0.78	0.12
II–10	50.0	0.82	19.3	10.3	0.18	4.2	9.1	2.4	0.99	0.05
2–1	75.3	0.21	13.0	2.0	0.05	0.6	3.5	3.3	2.15	0.01
2–2	62.0	0.79	15.4	8.4	0.17	2.1	5.9	3.5	1.24	0.01
2–3	61.9	0.71	14.7	8.4	0.13	2.0	5.7	3.6	1.03	0.01
2–4	75.3	1.70	11.3	21.2	0.29	1.7	4.9	2.7	0.98	0.01
2–5	57.1	0.84	17.8	7.9	0.18	3.4	3.3	4.4	1.77	0.04
2–6	59.4	0.66	17.4	7.4	0.13	2.8	5.9	3.8	1.76	0.06
2–7	58.8	0.67	16.8	7.7	0.17	2.9	6.2	3.6	1.61	0.04
2–8	61.5	0.61	16.9	6.7	0.07	2.3	5.6	3.7	2.11	0.04
2–9	61.0	0.82	15.8	7.8	0.12	3.3	1.4	4.5	1.94	0.05
2–10	58.4	0.74	17.0	7.9	0.16	3.0	6.6	3.7	1.52	0.03
3–1	58.6	0.72	17.0	7.4	0.17	2.9	6.2	3.8	1.66	0.03
3–2	59.2	0.69	16.9	7.4	0.16	2.9	6.4	3.7	1.61	0.03
3–3	59.4	0.66	17.0	7.1	0.14	2.7	6.6	3.7	1.55	0.02
3–5	59.0	0.72	16.9	7.4	0.16	2.8	6.5	3.8	1.60	0.03
3–6	59.7	0.63	16.8	7.4	0.15	2.7	6.3	3.7	1.59	0.04
3–7	59.4	0.72	16.9	7.3	0.17	3.0	6.4	3.8	1.60	0.03
3–8	59.1	0.69	16.5	7.5	0.17	3.0	6.1	3.6	1.65	0.03
3–9	58.1	0.69	17.4	7.7	0.15	3.0	6.7	3.7	1.45	0.03
3–10	60.1	0.71	16.6	7.2	0.15	2.7	6.1	3.8	1.77	0.02
4–1	60.2	0.82	14.3	9.8	0.18	2.4	5.4	3.2	1.58	0.01
4–2	62.9	1.19	12.6	12.0	0.16	1.4	5.3	3.2	1.57	0.01
4–3	60.1	0.81	12.2	11.4	0.11	3.3	5.0	3.0	1.82	0.01
4–4	57.8	0.73	16.6	8.3	0.20	3.3	6.5	3.4	1.81	0.02
4–5	61.2	0.78	15.8	7.3	0.14	2.7	5.3	3.6	2.21	0.02
4–6	60.0	0.72	15.6	8.1	0.12	3.1	5.4	3.5	2.34	0.03
4–7	58.8	0.62	16.9	7.8	0.09	3.0	6.3	3.6	1.80	0.02
4–8	58.7	0.73	16.2	7.9	0.15	3.2	5.8	3.4	1.88	0.07
4–9	59.2	0.72	16.6	8.0	0.17	3.2	6.3	3.7	1.72	0.04
4–10	58.0	0.69	16.7	8.2	0.14	3.1	6.4	3.5	1.70	0.05
MOR 98–0	58.0	0.73	17.0	8.6	0.16	3.2	6.4	3.2	1.49	0.18
MOR 98–2	58.9	0.65	16.4	7.4	0.12	2.8	6.2	3.4	1.89	0.17
MOR 98–3	57.0	0.67	16.7	8.4	0.15	3.0	7.1	3.3	1.54	0.19
MOR 98–4	58.1	0.72	16.3	8.6	0.15	3.1	6.1	3.6	1.45	0.19
MOR 98–5	56.5	0.71	16.7	8.3	0.16	3.1	6.2	3.3	1.68	0.17

Table B4: Purdue PRIME Lab AMS data and input variables.

Sample ID	Weight (g)	Weight added spike (mg)	$^{36}Cl/Cl$ (x 10^{-15})	$^{35}Cl/$ ^{37}Cl	Error (%)	Cl (ppm)	Conc. ^{36}Cl (atoms/g)	^{36}Cl uncertainty
I–2	30.00	1.02	388 ± 16	19.4	4.1	1.4	237513	9794
I–3	30.01	1.04	750 ± 100	14.6	13.3	5.1	550199	73360
I–4	27.33	1.01	402 ± 17	17.3	4.3	1.1	316617	13513
I–6	23.41	1.01	278 ± 29	18.7	10.4	0.3	249605	25839
I–7	25.97	1.00	273 ± 12	9.2	4.3	16.1	288687	12540
I–8	25.90	1.00	274 ± 11	8.8	4.1	18.1	300257	12178
I–9	22.77	1.01	259 ± 11	7.7	4.3	28.2	354606	15301
I–10	21.33	1.01	402 ± 15	17.5	3.7	1.3	405835	14975
II–2	30.09	1.02	19 ± 3	3.2	15.2	8.2	224906	34266
II–5	30.15	1.01	715 ± 298	16.7	41.6	2.9	520733	216769
II–6	26.14	1.00	493 ± 33	17.2	6.7	2.8	403995	27097
II–8	23.49	1.01	345 ± 13	12.9	3.8	8.9	348130	13358
II–9	21.74	1.00	373 ± 14	16.6	3.8	4.1	371667	14304
II–10	30.07	1.02	480 ± 26	18.2	5.5	2.0	346033	19036
2–1	30.02	1.03	334 ± 29	3.9	8.7	174.6	1010266	87718
2–2	30.00	1.01	175 ± 9	3.7	5.1	260.2	593425	30519
2–3	30.01	1.03	208 ± 11	3.8	5.3	218.0	657242	34758
2–4	24.85	1.04	207 ± 11	4.3	5.3	134.4	464668	24693
2–5	25.46	1.01	189 ± 19	5.0	10.2	75.4	380778	38794
2–6	25.63	1.02	189 ± 8	3.7	4.4	295.6	1048430	46205
2–7	25.26	1.02	179 ± 8	3.5	4.5	239.9	834428	37585
2–8	25.56	1.00	162 ± 7	3.6	4.2	347.4	1023950	42988
2–9	25.48	1.01	197 ± 10	5.0	4.9	76.2	401335	19556
2–10	25.45	1.01	142 ± 8	3.5	5.5	405.7	1020543	56463
3–1	25.77	1.03	147 ± 9	3.5	5.8	393.2	1031158	60164
3–2	25.71	1.00	86 ± 10	3.4	11.2	507.8	709430	79551
3–3	25.24	1.01	156 ± 9	3.8	5.6	256.2	758216	42752
3–5	25.27	1.00	164 ± 9	3.6	5.2	349.8	1044610	54336
3–6	25.55	1.00	139 ± 8	3.5	5.4	456.7	1106328	59707
3–7	25.24	1.00	141 ± 7	3.5	5.2	399.1	999280	51868
3–8	25.22	1.00	161 ± 8	3.6	5.1	327.2	964233	48865
3–9	25.25	1.01	171 ± 9	3.7	5.3	276.7	891959	47329
3–10	25.25	1.01	152 ± 8	3.5	5.5	425.5	1145305	62885
4–1	30.12	1.01	802 ± 27	3.6	3.4	321.7	4574836	154016
4–2	30.01	1.01	123 ± 4	3.5	3.3	339.0	412998	13431
4–3	30.01	1.04	234 ± 7	3.5	3.0	367.3	1216246	36383
4–4	25.24	1.00	328 ± 14	3.5	4.4	397.6	2415086	106040
4–5	25.18	1.01	336 ± 13	3.7	3.9	284.9	1856938	72632
4–6	25.43	1.03	219 ± 12	3.7	5.4	268.5	1132525	60840

Table B4. Continued

Sample ID	Weight (g)	Weight added spike (mg)	$^{36}Cl/Cl$ (x 10^{-15})	$^{35}Cl/$ ^{37}Cl	Error (%)	Cl (ppm)	Conc. ^{36}Cl (atoms/g)	^{36}Cl uncertainty
4–7	25.60	1.01	158 ± 9	3.6	5.8	348.9	998119	58053
4–8	25.28	1.01	237 ± 9	3.9	4.0	194.8	943652	37521
4–9	25.33	1.01	271 ± 14	4.4	5.1	123.1	767176	39422
4–10	25.29	1.01	295 ± 15	3.9	5.2	196.4	1192312	61587
MOR 98–0	40.06	1.03	305 ± 15	4.6	4.9	64.0	488849	24042
MOR 98–2	40.05	1.03	154 ± 6	3.4	3.9	382.3	1015314	39558
MOR 98–3	40.08	1.02	293 ± 9	4.4	3.1	78.4	537189	16501
MOR 98–4	40.02	1.06	310 ± 25	4.2	8.1	89.1	628409	50678
MOR 98–5	40.04	1.06	427 ± 11	4.0	2.6	123.1	1115174	28728

Table B5: Cosmogenic ^{36}Cl exposure ages using different erosion rates and the Desilets and Zreda scaling model (Desilets and Zreda, 2003; Desilets et al., 2006).

	Desilets and Zreda (Desilets and Zreda, 2003; Desilets et al., 2006) Scaling Model							
	Erosion Rate							
	0 mm/kyr		1 mm/kyr		2 mm/kyr		3 mm/kyr	
Sample ID	Age (ka)	Uncertainty (ka)	Age (ka)	Uncertainty (ka)	Age (ka)	Uncertainty (ka)	Age (ka)	Uncertainty (ka)
I–2	13.6	2.2	13.7	2.2	13.7	2.2	13.7	2.2
I–3	41.1	5.9	41.0	6.0	41.4	6.1	41.5	6.2
I–4	14.0	2.5	14.1	2.5	14.1	2.5	14.1	2.5
I–6	10.2	2.3	10.2	2.3	10.2	2.3	10.3	2.4
I–7	12.0	2.0	12.0	2.0	12.0	2.0	12.0	2.0
I–8	10.7	1.8	10.7	1.8	10.7	1.8	10.7	1.8
I–9	21.6	3.2	21.5	3.1	21.0	3.0	21.0	3.0
I–10	13.4	2.6	13.5	2.6	13.5	2.6	13.6	2.6
II–2	7.5	1.8	7.5	1.8	7.5	1.8	7.5	1.8
II–5	18.8	7.1	18.8	7.1	18.9	7.1	19.0	7.1
II–6	14.8	2.3	14.9	2.4	14.9	2.4	14.9	2.4
II–8	14.1	2.1	14.1	2.1	14.1	2.1	14.1	2.1
II–9	12.7	2.2	12.7	2.2	12.8	2.2	12.8	2.2
II–10	12.0	2.0	12.0	2.0	12.0	2.0	12.3	2.1
2–1	15.1	3.1	15.0	3.1	14.8	3.1	15.0	3.0
2–2	7.0	1.4	7.0	1.4	6.9	1.3	6.9	1.3
2–3	9.4	2.4	9.3	2.4	9.2	2.4	9.2	2.4
2–4	10.6	2.1	10.6	2.1	10.5	2.1	10.5	2.1
2–5	10.6	2.2	10.6	2.1	10.5	2.1	10.5	2.2
2–6	11.4	2.7	11.3	2.7	11.2	2.7	11.2	2.7
2–7	10.7	2.5	10.7	2.5	10.6	2.5	10.5	2.5
2–8	9.9	2.6	9.8	2.6	9.7	2.6	9.6	2.6
2–9	11.8	2.1	11.7	2.1	11.7	2.1	11.6	2.1
2–10	8.4	2.3	8.4	2.3	8.3	2.2	8.3	2.2
3–1	9.1	2.6	9.1	2.6	9.0	2.5	8.9	2.5
3–2	5.3	1.2	5.3	1.2	5.2	1.2	5.2	1.2
3–3	9.1	2.3	9.0	2.3	9.0	2.3	8.9	2.3
3–5	10.4	2.8	10.3	2.7	10.2	2.7	10.2	2.7
3–6	8.7	2.5	8.6	2.5	8.6	2.4	8.5	2.4
3–7	8.8	2.5	8.8	2.4	8.7	2.4	8.6	2.4
3–8	10.1	2.7	10.0	2.6	9.9	2.6	9.8	2.6
3–9	10.7	2.7	10.6	2.6	10.5	2.6	10.4	2.6
3–10	9.7	2.8	9.6	2.8	9.5	2.8	9.5	2.7
4–1	48.0	13.0	46.0	12.0	45.0	9.8	44.0	9.0
4–2	5.1	1.0	5.0	1.0	5.0	1.0	5.0	1.0
4–3	13.7	3.2	13.6	3.1	13.4	3.1	13.3	3.1

Table B5. Continued

Desilets and Zreda (Desilets and Zreda, 2003; Desilets et al., 2006) Scaling Model
Erosion Rate

Sample ID	0 mm/kyr		1 mm/kyr		2 mm/kyr		3 mm/kyr	
	Age (ka)	Uncertainty (ka)	Age (ka)	Uncertainty (ka)	Age (ka)	Uncertainty (ka)	Age (ka)	Uncertainty (ka)
4–4	22.5	4.9	22.1	4.7	21.8	4.4	21.6	4.2
4–5	21.8	4.1	21.5	3.9	21.3	3.7	21.1	3.6
4–6	15.6	3.1	15.0	3.0	15.4	2.9	15.3	2.9
4–7	10.5	2.8	10.4	2.7	10.4	2.7	10.3	2.7
4–8	14.8	2.7	14.7	2.7	14.6	2.7	14.5	2.7
4–9	15.4	2.5	15.3	2.5	15.3	2.4	15.2	2.4
4–10	18.4	3.3	18.3	3.3	18.1	3.3	18.0	3.4
MOR 98–0	11.9	1.8	11.9	1.8	11.8	1.8	11.8	1.8
MOR 98–2	9.0	2.4	8.9	2.4	8.8	2.4	8.8	2.3
MOR 98–3	11.8	1.8	11.8	1.8	11.7	1.7	11.7	1.8
MOR 98–4	14.0	2.3	13.9	2.3	13.9	2.4	13.9	2.3
MOR 98–5	19.2	2.6	19.1	2.6	19.0	2.7	18.9	2.7

Table B6: Cosmogenic ^{36}Cl exposure ages using different erosion rates and the Lifton and Sato scaling model (Lifton et al, 2008; Sato et al., 2008; Lifton et al., 2014).

	Lifton and Sato (Lifton et al., 2008; Sato et al., 2008; Lifton et al., 2014) Scaling Model							
	Erosion Rate							
	0 mm/kyr		1 mm/kyr		2 mm/kyr		3 mm/kyr	
Sample ID	Age (ka)	Uncertainty (ka)	Age (ka)	Uncertainty (ka)	Age (ka)	Uncertainty (ka)	Age (ka)	Uncertainty (ka)
I–2	15.3	0.9	15.3	0.9	15.4	0.9	15.4	1.0
I–3	43.1	5.3	43.2	5.4	43.4	5.5	43.5	5.6
I–4	16.2	1.2	16.3	1.2	16.3	1.2	16.4	1.2
I–6	12.0	1.4	12.0	1.4	12.0	1.4	12.1	1.5
I–7	13.6	1.1	13.6	1.1	13.6	1.1	13.6	1.1
I–8	12.3	0.9	12.3	0.9	12.3	0.9	12.3	0.9
I–9	22.3	2.2	22.2	2.2	22.1	2.1	22.0	2.1
I–10	15.7	1.1	15.8	1.2	15.8	1.2	15.7	1.1
II–2	8.9	1.7	8.9	1.7	8.9	1.7	8.9	1.7
II–5	20.8	6.6	20.9	6.7	20.9	6.8	21.0	7.0
II–6	16.8	1.4	16.9	1.4	16.9	1.4	17.0	1.4
II–8	16.0	1.0	16.0	1.0	16.0	1.0	16.0	1.0
II–9	14.6	0.9	14.7	0.9	14.7	0.9	14.8	0.9
II–10	14.0	1.0	14.0	1.1	14.0	1.1	14.0	1.1
2–1	17.1	2.8	16.9	2.8	16.7	2.8	16.6	2.8
2–2	8.1	1.6	8.0	1.5	8.0	1.5	7.9	1.5
2–3	11.0	2.1	10.9	2.1	10.8	2.1	11.0	2.0
2–4	12.0	1.7	11.9	1.6	11.9	1.67	11.8	1.6
2–5	11.8	1.7	11.7	1.7	11.7	1.8	11.6	1.7
2–6	13.2	2.4	13.0	2.4	12.9	2.3	12.8	2.3
2–7	12.4	2.1	12.0	2.0	12.0	2.0	12.0	2.0
2–8	11.5	2.2	11.4	2.2	11.3	2.1	11.2	2.1
2–9	12.9	1.7	12.8	1.7	12.7	1.6	12.7	1.7
2–10	10.0	2.2	9.9	2.2	9.8	2.2	10.0	2.2
3–1	10.7	2.3	10.6	2.3	10.5	2.2	10.4	2.2
3–2	5.9	1.0	5.9	1.0	5.9	1.0	5.8	0.9
3–3	10.6	2.1	10.5	2.1	10.0	2.0	10.4	1.9
3–5	12.1	2.3	12.0	2.2	11.9	2.2	11.8	2.2
3–6	10.3	2.3	10.2	2.2	10.1	2.2	10.0	2.2
3–7	10.4	2.2	10.3	2.2	10.2	2.1	10.1	2.2
3–8	11.7	2.2	11.6	2.3	11.5	2.2	11.4	2.2
3–9	12.4	2.1	12.3	2.1	12.1	2.1	12.0	2.0
3–10	11.3	2.4	11.2	2.3	11.1	2.3	11.3	2.4
4–1	54.0	12.0	52.0	12.0	50.0	11.0	50.0	10.0
4–2	5.6	0.7	5.6	0.7	5.6	0.7	5.6	0.7
4–3	15.4	2.5	15.3	2.4	15.1	2.3	15.0	2.3

Table B6. Continued

Lifton and Sato (Lifton et al., 2008; Sato et al., 2008; Lifton et al., 2014) Scaling Model

Erosion Rate

| Sample ID	0 mm/kyr		1 mm/kyr		2 mm/kyr		3 mm/kyr	
	Age (ka)	Uncertainty (ka)	Age (ka)	Uncertainty (ka)	Age (ka)	Uncertainty (ka)	Age (ka)	Uncertainty (ka)
4–4	25.0	3.8	24.6	3.8	24.2	3.7	23.9	3.9
4–5	24.1	3.5	23.8	3.5	23.4	3.5	23.1	3.5
4–6	17.5	2.5	17.3	2.5	17.1	2.5	17.0	2.5
4–7	12.2	2.2	12.0	2.2	11.9	2.2	11.8	2.2
4–8	16.7	2.4	16.5	2.4	16.4	2.4	16.3	2.4
4–9	17.3	2.1	17.2	2.1	17.0	2.0	17.0	2.0
4–10	20.3	2.3	20.1	2.2	20.0	2.2	20.3	2.3
MOR 98–0	13.5	1.4	13.5	1.4	13.4	1.3	13.4	1.4
MOR 98–2	10.6	2.2	10.5	2.2	10.4	2.1	10.3	2.1
MOR 98–3	13.4	1.2	13.4	1.3	13.4	1.3	13.3	1.3
MOR 98–4	16.0	2.0	15.7	1.9	15.7	1.9	15.6	1.9
MOR 98–5	21.1	1.9	21.0	1.9	20.9	1.8	20.7	1.8
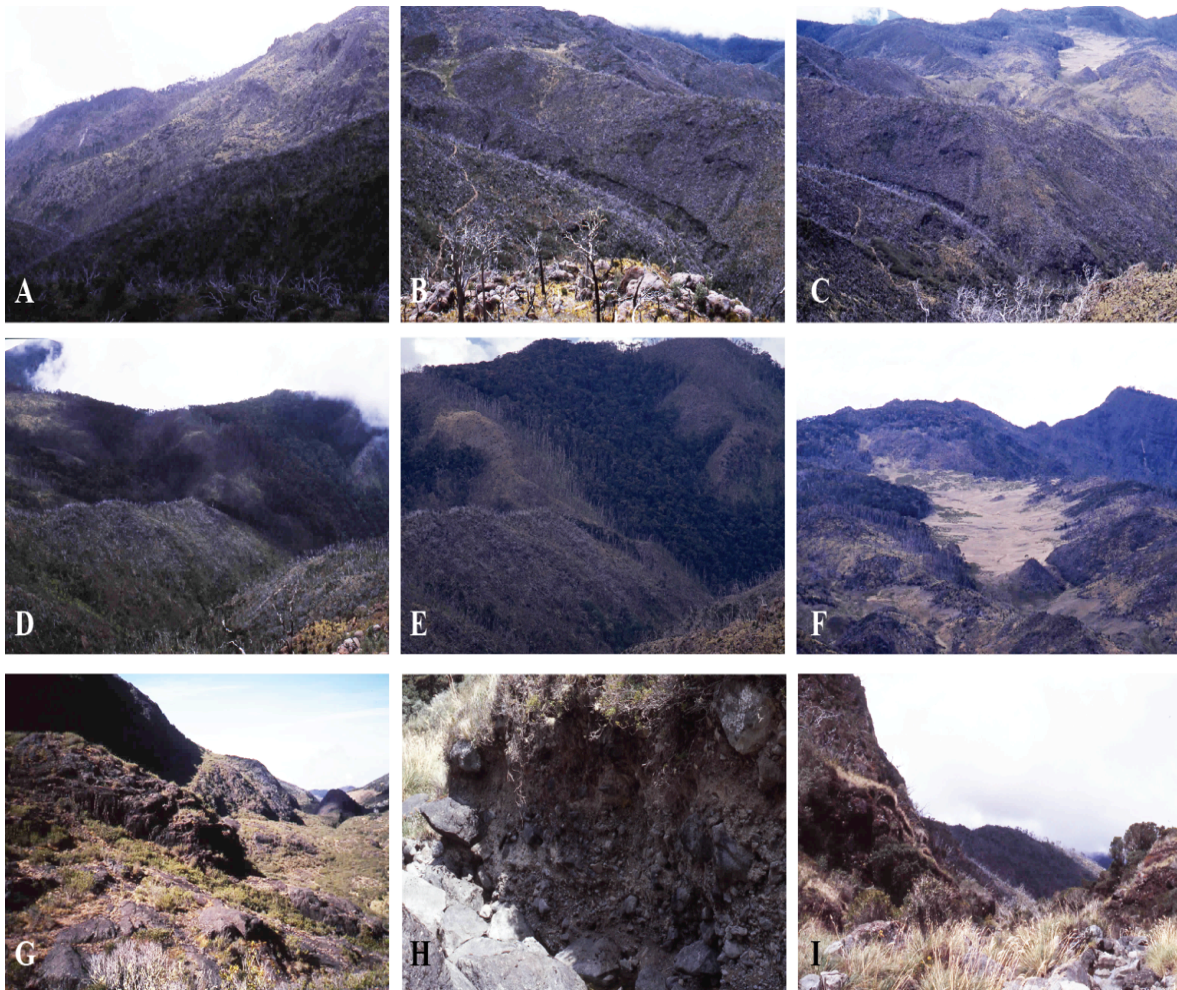
Figure B1: Images of moraines and glacial features in the Talari Valley. (A) Talari moraine surface in basin; (B) Talari moraines; (C) Talari moraines and Sabana Leones; (D) big Talari moraine; (E) gash near downstream of big Talari moraine; (F) Sabana Leones; (G) breach below Crestones; (H) breached Talari moraine; (I) through breached moraine to lower moraine in the Talari Valley.

VITA

Rebecca Potter was born and raised in Cincinnati, Ohio. She received her Bachelors of Science in Geology from the University of Cincinnati in Cincinnati, Ohio in 2012. Her love for geology developed as a young child during annual backpacking trips with her father in the deserts of the southwestern U.S.A.. She transferred from environmental sciences to geology her second year in college when she took an introduction to geology class and realized that she could simultaneously pursue her true passion and career. She developed a great interest in Quaternary geology and began working as an undergraduate laboratory assistant in the Cosmogenic Nuclide Laboratory run by Dr. Lewis A. Owen in the Department of Geology. Throughout her undergraduate career, she was fortunate to go on many geological field trips including a three-week course across the Himalayas, a structural/tectonics trip to the Mecca Hills, California, and a five-week capstone field camp through Southern Utah University in Cedar City, Utah.

Rebecca began her Master's work at the University of Tennessee in 2012 under the advisement of Dr. Yingkui Li. There she helped to set up a cosmogenic laboratory where she processed her own samples from Costa Rica and supervised other colleagues in processing their own cosmogenic samples. Her research focused on establishing a glacial chronology in the Cordillera de Talamanca, Costa Rica using cosmogenic ^{36}Cl nuclide surface exposure dating.